齒醫科學博士學位論文

Novel roles of S100A4 in the pathogenesis of rheumatoid arthritis and bone metastasis

류마티스성 관절염과 골 전이암 발병에서의 S100A4의 역할

2017년 2월

서울대학교 대학원

치의과학과 세포및발생생물학 전공

김해민

Novel roles of S100A4 in the pathogenesis of rheumatoid arthritis and bone metastasis

by

Haemin Kim

Advisor:

Prof. Hong-Hee Kim, Ph.D

A Thesis Submitted in Partial Fulfillment of the
Requirements for the Degree of Doctor of Philosophy

February, 2017

Division of Cell and Developmental Biology
Department of Dental Science, School of Dentistry
Seoul National University

류마티스성 관절염과 골 전이암 발병에서의 S100A4 의 역할

지도교수 김홍희

이 논문을 치의과학박사학위논문으로 제출함

2016 년 10 월

서울대학교 대학원

치의과학과 세포및발생생물학 전공

김해민

김해민의 박사학위논문으로 인준함

2016 년 12 월

위 원 장 _____(인)

부위원장 _____(인)

위 원 _____(인)

위 원 _____(인)

위 원 _____(인)

Novel roles of S100A4 in the pathogenesis of rheumatoid arthritis and bone metastasis

by

Haemin Kim

Advisor:

Prof. Hong-Hee Kim, Ph.D

A Thesis Submitted in Partial Fulfillment of the
Requirements for the Degree of Doctor of Philosophy

December, 2016

Doctoral Committee:

Professor _____, Chairman
Professor _____, Vice chairman
Professor _____
Professor _____
Professor _____

ABSTRACT

Novel roles of S100A4 in the pathogenesis of rheumatoid arthritis and bone metastasis

Haemin Kim

Division of Cell and Developmental Biology

Department of Dental Science

Seoul National University

(Directed by Prof. Hong-Hee Kim, Ph.D)

S100A4 is a member of the S100 calcium-binding protein family which has been implicated in various pathological conditions including cancers and arthritis, which often accompany bone destruction. Recently, the roles of S100A4 in progression of cancer metastasis and rheumatoid arthritis (RA) have been demonstrated in several studies. However, how S100A4 affects the bone microenvironment during pathogenesis of RA and bone metastasis has not been

elucidated. Based on the results of ELISA, S100A4 was highly expressed in synovial fluid of RA patients. Interestingly, in silico analyses demonstrated that the expression of S100A4 was maintained in RA patients even after TNF-alpha inhibitor treatment. Moreover, breast cancer patients with bone metastases expressed elevated levels of S100A4 by searching publicly available data sets. In line with that finding, in vivo selection of bone metastasized prostate and breast cancer in athymic mice showed increased expression of S100A4.

In this study, I demonstrated in vivo and in vitro that the extracellular S100A4 proteins decreased the bone volume of mice calvariae, resulting from enhancement of osteoclastogenesis and interruption of osteoblast function. I observed that the receptor for advanced glycation end products (RAGE), a direct binding target of S100A4, mediated osteoclastogenesis via activation of classical NF-κB signaling pathways upon S100A4 treatment. Moreover, the extracellular S100A4 inhibited the mineralization by osteoblasts by activating the NF-κB pathway. Additionally, synovial fibroblasts from RA patients expressed high levels of receptor activator of nuclear factor κB ligand (RANKL), a potent cytokine of osteoclastogenesis, upon S100A4 treatment. These results demonstrated the bone destructive effect of extracellular S100A4 in bone homeostasis and suggested a novel therapeutic target to cure bone metastasis and RA.

Key words: S100A4, osteoclast, osteoblast, bone metastasis, and rheumatoid arthritis

***Student Number*:** 2015-30621

Contents

LIST OF FIGURES

LIST OF ABBREVIATIONS

ALP, alkaline phosphatse

Ab., antibodies

α–MEM, α-minimum essential medium

BMM, bone marrow-derived macrophage

mtMDA, bone metastasized MDA

mtPC3, bone metastasized PC3

BMP, bone morphogenetic protein

BMP2, bone morphogenetic protein 2

BSA, bovine serum albumin

CM, conditioned medium

DAPI, 4',6-diamidino-2-phenylindole

ELISA, enzyme-linked immunosorbent assay

EMT, epithelial to mesenchymal transition

EDTA, ethylenediaminetetraacetic acid

ERK, extracellular signal-regulated kinase

GEO, gene expression omnibus

H&E, hematoxylin & eosin.

hHLA, human leukocyte antigens

HPRT, hypoxanthine-guanine phosphoribosyltransferase

IGF-1, insulin-like growth factor 1

IL, interleukin

JNK, c-Jun N-terminal kinase

KO, knock-out

M-CSF, macrophage colony-stimulating factor

M, M-CSF

MDA, MDA-MB-231

MMP, metalloproteinase

μCT, microcomputed tomography, micro-CT

MAPK, mitogen-activated protein kinase

MAR, mineral apposition rate

NCBI, national center for biotechnology information

NMMHC, non-muscle myosin heavy chain

N.S., not significant

NF-κB, nuclear factor κB

NFATc1, nuclear factor of activated T-cells c1

OA, osteoarthritis

OPG, osteoprotegerin

PTHrP, parathyroid hormone-related protein

Pt., patient

pOC, pre-fusion osteoclast

PCR, polymerase chain reaction

R, RANKL

RANKL, receptor activator of NF-κB ligand

RAGE, receptor for advanced glycation end products

RT-PCR, reverse transcription PCR

RA, rheumatoid arthritis

SDS, sodium dodecyl sulfate

SF, synovial fluid

TRAP, tartrate-resistant acid phosphastase

TGF-β, transforming growth factor-beta

TNF-α, tumor necrosis factor-aplha

TLR4, toll-like receptor 4

Veh, vehicle

CHAPTER 1

INTRODUCTION

Osteoporosis, characterized by increased bone fragility due to inadequate bone mass and/or bone microarchitecture, is a very common disease in the elderly, affecting more than 10 million Americans at present (1). An imbalance of bone resorption by osteoclasts and bone formation by osteoblasts in bone homeostasis is the main pathophysiology of osteoporosis (2). Moreover, osteoporosis gets more complicated when inflammatory conditions, such as arthritis and cancer, are accompanied. Therefore, osteoporosis is a global concern, not only limited to the elderly but also to individuals who have inflammatory diseases.

In order to tackle osteoporosis, in-depth understanding of bone remodeling has been a major subject of bone biology field. Accumulating evidence suggested that the bone is constantly remodeled in mammals including human. Accordingly, bone homeostasis is under control of tight regulations between bone resident cells. Most importantly, bone catabolism and anabolism must be well-balanced to sustain the proper bone homeostasis. Three steps in bone remodeling have been suggested: (a) initiation, osteoclast resorbs old or damaged bones; (b) reversal, osteoblast is recruited to the resorbed bone surface; (c) formation, osteoblast deposits new bone to the resorbed area (3). Imbalance of a certain step in bone remodeling jeopardizes the bone homeostasis, thus operation of three steps should be well characterized in details.

Two key players of bone homeostasis, osteoclast and osteoblast, will be mainly discussed throughout this thesis. Osteoclast, a cell responsible for bone resorption, is originated from macrophage/monocyte lineage of hematopoietic stem cells. Osteoclastogenesis, a process of osteoclast differentiation, is supported by two critical key cytokines, macrophage colony-stimulating factor (M-CSF) and receptor activator of nuclear factor κB (NF-κB) ligand (RANKL) (4, 5). M-CSF is responsible for proliferation and survival of osteoclast precursors, whereas RANKL induces osteoclast differentiation from the precursors and activation of osteoclasts (6, 7). Additionally, RANKL activates various transcription factors to finely orchestrate osteoclast differentiation and activation (4). Particularly, nuclear factor-activated T cells c1 (NFATc1) has long been studied as a master regulator of osteoclastogenesis, regulating several genes necessary for osteoclast differentiation (8, 9). NF-κB and c-Fos also play pivotal roles in cooperation with NFATc1 to mediate osteoclast differentiation (9). On the other hand, the anabolism of bone is mainly mediated by deposition of mineralized matrix from osteoblasts. Osteoblasts are originated from bone marrow mesenchymal stem cells (10). The formation of osteoblast is supported by bone morphogenetic proteins (BMPs), Wnts, and transforming growth factor-beta (TGF-β) signaling pathways. Ultimately, various transcription factors such as Runx2, osterix, and β-catenin induce expression of genes required for bone formation (11-13). Taken together,

understanding molecular mechanisms and networks between bone cells envisions strategies against bone-destructive diseases.

Rheumatoid arthritis (RA) is an autoimmune disease resulting in inflamed joints with eventual bone erosions, followed by chronic pain. The inflamed joint is a rich reservoir for cytokines and proteolytic enzymes that directly or indirectly stimulate stromal cells residing in the synovial joint. Over-activated macrophages, and T and B lymphocytes accumulate in the synovial lining, eventually damaging the cartilages and the subarticular bones (14-17). Especially, synovial fibroblasts become stimulated by proinflammatory cytokines such as tumor necrosis factor-aplha (TNF-α), interleukin (IL)-1β, and IL-6 to secrete soluble and express more membrane bound RANKL to differentiate and activate bone resorbing osteoclasts (Figure 1) (18).

Breast and prostate cancer are most invasive among cancers and they are almost incurable when metastasized in other organs. Moreover, most of breast and prostate cancer patients experience bone metastases and suffer from extreme pain and physical disabilities that dramatically lower the quality of life (19). Eventually, irresistible nerve pains, fragility bone fractures, and hypercalcemia lead most of bone-metastasized patients to death (20). Several groups of researchers and scientists are trying to find a cure, but no specific drug that targets bone metastasized tumors is yet to be developed. However, recent findings

enlighten the field of bone metastasis research which is well-described in a term, ‘vicious cycle.’ This concept explains how primary tumors accustomed to the bone microenvironment and proliferate in such environment (Figure 2) (20). In more details, disseminated cells from the primary site extravasate into the circulation and eventually enter the bone marrow via blood vessels, then the tumor cells secrete various kinds of cytokines such as interleukins, parathyroid hormone-related protein (PTHrP) and matrix degrading enzymes such as metalloproteinases (MMPs) (21). These cytokines stimulate cells reside in the bone microenvironment, for instance osteoclasts and osteoblasts, to collapse finely orchestrated bone homeostasis. Most of breast cancers and some prostate cancers favor catabolism of bone matrix by directly activating osteoclasts or by indirectly inducing RANKL from osteoblasts (22). Subsequently, excessive bone resorption causes TGF-β and other factors to be released from the bone matrix, which fuels cancers to sustain the vicious cycle (23). Bone metastasized cancers also can be described by ‘osteomimicry,’ which represents a phenomenon that cancers beginning to express genes that are specifically expressed in bone cells, for instance Runx2 and osteopontin (24, 25). This makes ultimately the cancers to adhere to the bone microenvironment.

S100 proteins are calcium-binding proteins comprised of more than 20 members and play important roles in inflammation, cytoskeleton dynamics,

enzyme activity, and cell growth and differentiation (26-28). Many studies have revealed the roles of S100 proteins in pathological conditions, especially in tumor progression and arthritis (28). For instance, S100A2, S100A4, S100A6, S100A7, and S100B were found to be differentially expressed in cancer cells, while S100A12 was detected at a high level in synovial tissues of arthritis patients (29). However, each of the S100 proteins is thought to have a specific role or as yet unidentified critical role(s) under certain circumstances. Notably, S100A8 has been shown to activate osteoclasts by interacting with toll-like receptor 4 (TLR4) (30).

Over the last decade, S100A4 has been linked to RA pathogenesis. Klingelhofer and colleagues reported that synovial tissues of RA patients express S100A4 (31). In addition, S100A4 was reported to stimulate MMP-13 secretion via receptor for advanced glycation end products (RAGE) in chondrocytes, resulting in cartilage degradation (32). A study demonstrated that S100A4 was widely expressed in proliferating synovial tissue, such as synovial fibroblasts and other stromal cells (25). S100A4 also plays important roles in tumor progression by increasing tumor cell migration and invasion and MMP secretion (33). Both intracellular and extracellular functions of S100A4 have been studied (Figure 3). Intracellularly, S100A4 binds to tumor suppressor protein p53, where it aids in tumor survival, and tumor cell migration is regulated through interactions with

non-muscle myosin II (20, 21). Extracellularly, S100A4 induces neurite outgrowth in astrocytes and angiogenesis in endothelial cells (22, 23). Moreover, extracellular S100A4 binds to cell surface receptors such as RAGE to activate NF-κB and mitogen-activated protein kinase pathways for tumor cell invasion and survival (34). Recently, the three-dimensional structures of human S100A4 were reported in calcium-bound state, which is an active form of S100A4 (35). Calcium-bound state has been shown to form homodimer, which eventually targets other binding partners to mediate tumor progression (36).

Recently, the NF-κB signaling pathway was reported to be a negative regulator of osteogenesis (37, 38). NF-κB activation by proinflammatory cytokines such as TNF-α in osteoblast precursors inhibits osteogenic differentiation (39). RAGE, a receptor of S100A4, was shown to mediate activation of NF-κB in endothelial cells, macrophages, and lymphocytes (40). A study by Ogawa et al. reported that osteoblastic cells expressed RAGE, and that the addition of high glucose with AGE, one of the ligands of RAGE, inhibited mineralization (41). On the other hand, RAGE knock-out BMMs demonstrated defects in RANKL-induced osteoclastogenesis and bone resorption, indicating a possible mechanism of RAGE-NF-κB mediated signaling in osteoclasts (42). Taken together, accumulating data suggests that S100A4 might signal through RAGE to activate the NF-κB signaling pathway and suppress osteogenesis. In this

study, I employed by various experimental strategies to illuminate S100A4 as a negative player of bone homeostasis.

In the first section of result, I investigated the role of extracellular S100A4 on osteoblasts. I demonstrated that extracellular S100A4 did not affect early osteoblast differentiation. However, it inhibited mineralization activity via activation of the NF-κB signaling pathway in osteoblasts. Also, in vivo injection of recombinant S100A4 onto calvariae of neonatal mice decreased the mineral apposition rate.

In the second part of result section, I dealt with the role of S100A4 in RA, particularly focusing on osteoclasts. I observed a high concentration of S100A4 in RA patients. Next, I demonstrated extracellular S100A4 stimulated osteoclast resorption activity and this was also reproduced by S100A4 injection in vivo. I also examined whether extracellular S1004 stimulated RANKL-induced osteoclastogenesis and osteoclast marker gene inductions. Furthermore, I demonstrated that S100A4 activated the NF-κB pathway, especially the classical pathway, via RAGE to enhance osteoclastogenesis. In addition, I observed that osteoclasts themselves secreted S100A4 to support RANKL-induced osteoclastogenesis. Finally, I showed that extracellular S100A4 induced RANKL expression from human RA synovial fibroblasts. Taken together, an increased concentration of extracellular S100A4 in RA not only enhances

osteoclastogenesis directly, but also supports the process indirectly by stimulating synovial fibroblasts to express more RANKL. This phenomenon eventually drives the bone homeostasis towards bone destruction, emphasizing the proinflammatory role of S100A4 in RA and suggesting S100A4 as a good target to treat RA.

In the last part of result, I studied the function of cancer-secreted S100A4 on osteoclasts. I established bone metastasized prostate and breast cancer cell lines by intracardiacly injecting PC3 and MDA-MB-231 into immune-deficient mice. Then, I selected cells that were colonized in the bone marrow. These in vivo selected cancers expressed more mesenchymal markers and higher osteoclastogenic potential than their parental cells. Moreover, I found that enhanced osteoclastogenesis was due to an increased S100A4 expression by bone metastasized cancers and this can be regulated by a cell surface receptor, RAGE, on osteoclasts. In agreement with my findings, enhanced expression of S100A4 in bone metastatic tumor samples of breast cancer patients was reported in the GSE 14020 of NCBI data base. Collectively, these findings indicate that bone metastasized cancer cells express elevated expression of S100A4 and this contributes to enhanced bone-destruction by osteoclasts.

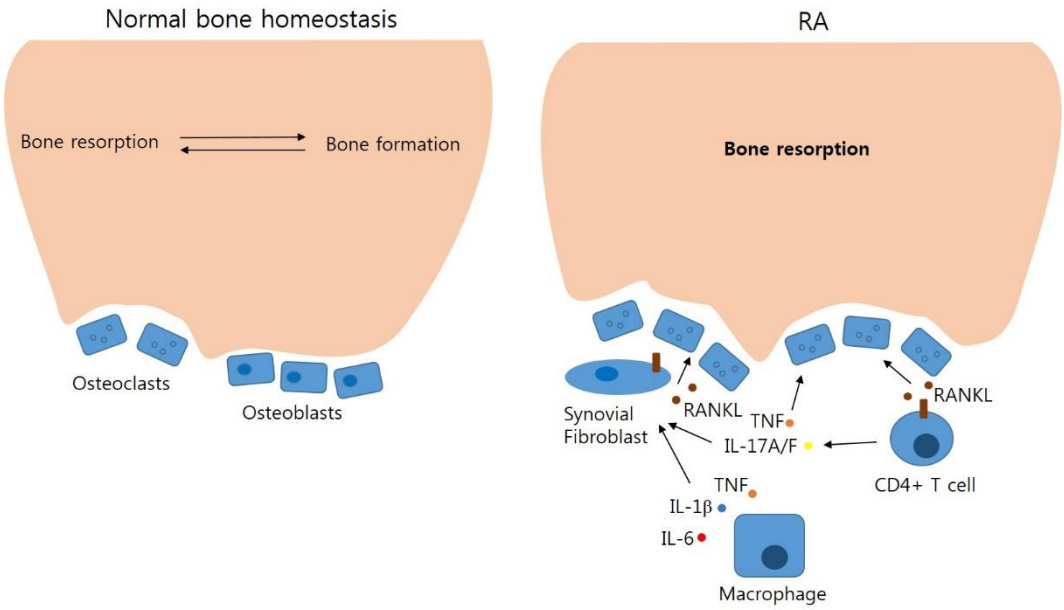

Modified from Choi et al. Nature Reviews Rheumatology, 2009

Figure. 1. Normal bone homeostasis vs. bone destruction in RA.

Bone homeostasis in normal condition is described by balanced resorption by osteoclasts and formation by osteoblasts. In RA condition, proinflammatory cytokines from CD4+ T cells and macrophages stimulate synovial fibroblasts to express RANKL, resulting increased bone resorption by osteoclasts.

IL, interleukin; RA, rheumatoid arthritis; RANKL, Receptor activator of NF-κB ligand; TNF, tumor necrosis factor

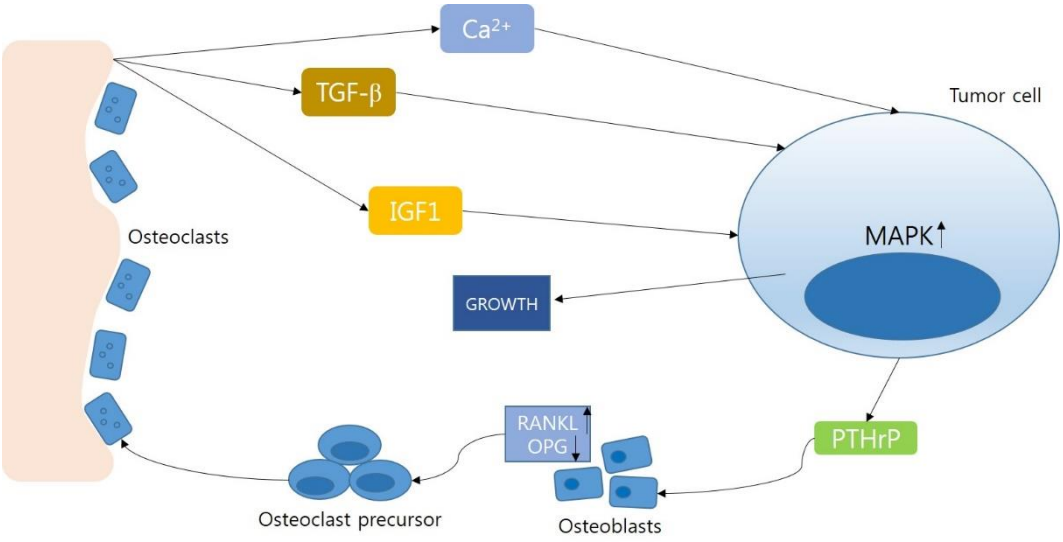

Modified from Mundy GR, Nature Reviews Cancer, 2002

Figure. 2. A schematic illustration explaining 'vicious cycle' theory.

After tumor cells enter the bone microenvironment, PTHrP is produced from tumor cells to stimulate osteoblasts to up-regulate RANKL and down-regulate OPG. This activates osteoclast precursors to differentiate into mature osteoclasts, eventually causing osteolysis. After all, growth factors stored in the bone matrix are released into the bone microenvironment, fueling tumor cells to produce more PTHrP. TGF-β, transforming growth factor-β; MAPK, mitogen-activated protein kinase; PTHrP, parathyroid-hormone-related peptide; RANKL, Receptor activator of NF-κB ligand; OPG, osteoprotegerin; IGF-1, insulin-like growth factor 1.

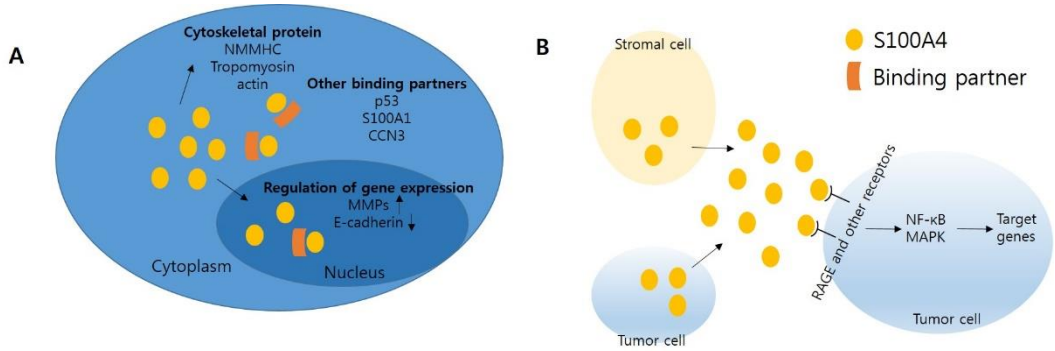

Modified from Boye and Maelandsmo, American Journal of Pathology, 2010

Figure. 3. The function of S1004 can be divided into intracellular and extracellular and they work independently to support the tumor progression. (A) Intracellular S100A4 interacts with NMHCA IIA, tropomyosin, and actin to support cell migration. Other binding partners of S100A4, including tumor suppressor protein p53, assist in tumor cell proliferation. Nuclear S100A4 is known to associate with transcriptional regulation of MMPs and E-cadherin. (B) Extracellular S1004, which is mainly secreted by stromal cells and tumor cells, binds to cell surface receptor such as RAGE to induce intracellular signaling activation of NF-κB and MAPK. NMMHC, non-muscle myosin heavy chain; MMP, metalloproteinase; RAGE, receptor for advanced glycation end products; MAPK, mitogen-activated protein kinase.

CHAPTER 2

MATERIALS AND METHODS

2.1 ANIMALS

Animal experiments were approved by the Committees on the Care and Use of Animals in Research at Seoul National University. All the animals were kept in an specific pathogen-free animal facility with consistent temperature (22℃) and humidity (55%), and a 12-hour light/dark cycle. The facility was operated by experienced animal handlers who were responsible for changing bedding material and providing food and sterilized water under the supervision of a veterinarian. 4 to 5 mice were housed in each cage. All the animals had free access to food and water. Before surgery, the animals were anesthetized by intraperitoneally injecting combinations of 2,2,2,-tribromoethanol and 2-methyl-2-butanol (1.2% avertin). The surgeries were performed in a clean bench stored in the specific pathogen-free facility. Animals were sacrificed in a carbon dioxide euthanasia chamber. Five-week-old female CrljOri:CD1 (ICR) mice (22±1 grams/mouse) were purchased from OrientBio (Sungnam, Korea) and used for bone marrow cell preparation. BMMs were prepared from the mice as previously described. For the recombinant mouse S100A4 calvarial injection model, 6 weeks old female ICR mice (n=5) were subcutaneously injected onto calvaria with 10 μg of S100A4 diluted in PBS (50 μl/injection) or an equal volume of vehicle diluted in PBS every other day for 8 days. One-day-old ICR mice were purchased from OrientBio and were used for in vitro calvarial osteoblast preparation and in vivo

experiments. Recombinant mouse S100A4 proteins (5 μg) diluted with PBS (45 μl) was injected onto the calvariae of 1-day-old mice (n=7 per group) at 3 days intervals starting on day 0. A total of 4 injections were performed (days 0, 3, 6, and 9). The mineral apposition rate was evaluated by intraperitoneally injecting 25 mg/kg calcein (dissolved in 2% $NaHCO_3$ and 150 mM NaCl) on days 6 and 10. Mice were sacrificed at day 12. The calvariae were embedded in methyl methacrylate (Merck) resins and tissue sections were visualized under a Zeiss LSM 700 laser-scanning microscope (Carl Zeiss Microimaging GmbH, Goettingen, Germany) to measure the distance between the initial and final calcein depositions. Pictures were taken and analyzed with the ZEN2010 program (version 6,0,0,320). Eight-week-old BALB/c-nude mice were purchased from OrientBio and used for in vivo selection of cancer cells. 10^4 to 10^5 cells of PC3 or MDA-MB-231 were injected intracardiacly into eight-week-old BALB/c-nude male or female mice. After 8 to 12 weeks, metastasized cells in femurs and tibiae were flushed out from the bone marrow and expanded in culture dishes for 2 months. Human cancer cells were validated by detecting human leukocyte antigens by FACS analyses. Mouse bone marrow cells were used as a negative control and HEK-293 cells were tested as a positive control. Then, bone metastasized cancers were re-injected intracardiacly, followed by another round of selection. These second rounds of selected cancers were named as mtPC3 and

mtMDA. Bone erosions were analyzed by scanning the femurs of mice injected with PBS or MDA-MB-231 or mtMDA-MB-231.

2.2. REAGENTS

Recombinant mouse S100A4 was purchased from Prospec (East Brunswick, NJ). Recombinant human M-CSF and human soluble RANKL were purchased from PeproTech (Rocky Hill, NJ). Recombinant OPG was purchased from R&D systems (Minneapolis, MN). Phosphospecific antibodies against ERK (Thr^{202}/Tyr^{204}), JNK (Thr^{182}/Tyr^{185}), p38 (Thr^{180}/Tyr^{182}), IKKα/β ($Ser^{176/180}$), IκB (Ser^{32}), p65 (Ser^{536}), Src (Tyr^{416}), ERK, JNK, p38, IKKα/β, IκB, Snail2, and p65 were obtained from Cell Signaling Technology (Beverly, MA). Antibodies against c-Fos, vimentin, Lamin B (M-20) and osterix were purchased from Santa Cruz Biotechnology, Inc. (Santa Cruz, CA). E-cadherin, N-cadherin, and NFATc1 (7A6) antibodies were obtained from BD Pharmingen (Franklin Lakes, NJ). Anti-β-actin(AC-74), β-glycerophosphate, ascorbic acid, polybrene, and calcein were purchased from Sigma. Antibodies for RAGE (DD/A11) were from Millipore (Billerica, MA). Anti-S100A4 was purchased from Abcam (Cambridge, UK). Anti-Runx2 was purchased from MBL International (Woburn, MA, USA). The leukocyte acid phosphatase (TRAP) kit and the alkaline phosphatse (ALP) kit were purchased from Sigma-Aldrich. The ALP assay kit for ALP activity

measurement was purchased from Takara Bio Inc. (Fukui, Japan). Lipofectamine2000 was purchased from Invitrogen for si-RNA transfection. Human S100A4 shRNA lentiviral particles and mouse RAGE si-RNAs were purchased from Santa Cruz Biotechnology, Inc. Mouse S100A4 ELISA kit was purchased from USCN (Hubei, China). Human S100A4 ELISA kit was purchased from CycLex Co., Ltd. (Nagano, Japan). Dentin slices were obtained from Immunodiagnostic Systems Inc. (Scottsdale, AZ, USA).

2.3. BONE MARROW-DERIVED MACROPHAGE (BMM) PREPARATION

The preparation of BMM from mice was described previously (43). Briefly, five-week-old female ICR mice were sacrificed for femur and tibia extraction. Bone marrow cells were flushed out by 1 ml syringe needles from extracted bones. Collected bone marrow cells were cultured in 100 mm culture dish for 24 hours. Cells that were not adhere to the culture dish were collected and re-seeded on 100 mm petri dish with M-CSF. After 4 days of incubation, adherent cells on the petri dish were collected with cell scrapers.

2.4. OSTEOCLAST DIFFERENTIATION

Mouse BMMs were seeded onto cell culture plates in α-minimum essential medium (α–MEM) containing M-CSF (30 ng/ml). The next day RANKL (100 ng/ml) was added and cells were cultured further with the medium changed every other day. For identification of osteoclasts, cells were stained for TRAP activity using the leukocyte acid phosphatase kit. TRAP-positive cells with 3 or more nuclei were considered to be mature osteoclasts. Cells were observed with an Olympus BX51 (Tokyo, Japan) and photographs were taken using DP2-BSW software provided by Olympus (version 2.2). Mature OCs were usually detected around 4~5 days after RANKL treatment for un-manipulated and siRNA-transfected BMMs and at day 6 for cells subjected to retroviral transduction. $TRAP^+$ pre-fusion OCs (pOCs) were usually detected around day 2~3 (for un-manipulated and siRNA-transfected BMMs) or day 4 (for virus-infected BMMs).

2.5. OSTEOCLAST RESORPTION ASSAY

A dentin slice was inserted into each well of 48-well tissue culture plates followed by seeding 4×10^4 BMMs. Seeded BMMs were cultured for 6 to 13 days in the presence of RANKL (100 ng/ml) and M-CSF (30 ng/ml). After removing the cells, dentin slices were washed with distilled water and mounted on glass slides. Samples were observed with a Zeiss LSM 5 PASCAL laser-scanning

microscope (Carl Zeiss Microimaging GmbH, Goettingen, Germany). Resorbed area and depth were calculated by the Zeiss LSM Image Browser program (version 3.0 SP3).

2.6. CALVARIAL OSTEOBLAST PREPARATION AND DIFFERENTIATION

Calvarial osteoblasts were prepared from 1-day-old mice as previously described (44). Prepared calvarial osteoblasts were seeded onto 48-well or 6-well cell culture plates in α–MEM (WELGENE, Daegu, Korea) supplemented with 10% fetal bovine serum (Invitrogen, Carlsbad, CA, USA). Osteogenic differentiation was induced by supplementing the culture media with 10 mM β-glycerophosphate and 100 μM ascorbic acid. For evaluation of osteoblast differentiation, ALP activity was measured using the ALP assay kit following the manufacturer's protocol. Mineralization was assessed after 10 days of culture by Alizarin-red staining as previously described (45), and the mean intensity was measured using the ImageJ program from the National Institutes of Health.

2.7. REAL-TIME PCR ANALYSIS

Quantification of mRNA expression by real-time PCR analysis was performed following a standard protocol. Primers for real-time PCR analysis are as follows: *runx2* forward, 5'-cgcacgacaaccgcacca-3'; *runx2* reverse, 5'-cagcacggagcacaggaagtt-3'; *bglap* forward, 5'-ccgggagcagtgtgagctta-3'; *bglap* reverse, 5'-tagatgcgtttgtaggcggtc-3'; *hprt* (hypoxanthine-guanine phosphoribosyltransferase) forward, 5'-cctaagatgagcgcaagttgaa-3'; *hprt* reverse, 5'- ccacagggactagaacacctgctaa-3' ; *atp6v0d2* reverse, 5'-ccaccgacagcgtcaaacaaa-3'; *mmp9* forward, 5'-gacggcacgccttggtgtag-3'; *mmp9* reverse, 5'-aggagcggccctcaaagatg-3'; *oscar* forward, 5'-gctgacttcacaccaacagc-3'; *oscar* reverse, 5'- gggtgacaaggccacttt-3'; *acp5* forward, 5'-cgaccattgttagccacatacg-3'; *acp5* reverse, 5'- tcgtcctgaagatactgcaggtt-3'; *ctsk* forward, 5'-atatgtgggccaccatgaaagtt-3'; *ctsk* reverse, 5'-tcgttccccacaggaatctct-3'; *dcstamp* forward, 5'-gggtgctgtttgccgctg-3'; *dcstamp* reverse, 5'-cgactccttgggttccttgct-3'; *s100a4* forward, 5'- ttggaggaggccctggatgt-3'; *s100a4* reverse, 5'-tccccaggaagctaggcagc-3'; human *hprt* forward, 5'- accccacgaagtgttggata-3'; human *hprt* reverse, 5'- aagcagatggccacagaact-3'; human *s100a4* forward, 5'-gcccagcttcttggggaaaa-3'; human *s100a4* reverse, 5'- atggcgatgcaggacaggaa-3'; human *rankl* forward, 5'- tcgttggatcacagcacatca-3'; human *rankl* reverse, 5'-tatgggaaccagatgggatgtc-3'. All the sequences are mouse unless indicated.

2.8. WESTERN BLOTTING

Cells were washed with cold PBS and lysed with RIPA buffer (10 mM Tris pH 7.2, 150 mM NaCl, 0.1% sodium dodecyl sulfate (SDS), 1% Triton X-100, 1% sodium deoxycholate, 5 mM ethylenediaminetetraacetic acid (EDTA)). Western blotting was performed with cell lysates following a standard protocol.

2.9. IMMUNOFLUORESCENCE MICROSCOPY

BMMs seeded on 12-mm microscope cover glass were differentiated to pre-fusion osteoclasts by culturing in the presence of M-CSF (30 ng/ml) and RANKL (100 ng/ml) for 2 days. Calvarial osteoblasts seeded on 12-mm microscope cover glass were incubated overnight. pOCs or calvarial osteoblasts were serum-starved for 5 hours, followed by stimulation with mouse recombinant S100A4 (2 μg/ml) for an hour. Cells were fixed with 3.7% formaldehyde, and permeabilized with 0.1% Triton X-100 for 15 minutes. After blocking non-specific sites with 1% bovine serum albumin (BSA)-PBS for 2 hours, cells were incubated with anti-p65 (1/100 dilution) for overnight and anti-lamin B (1/50 dilution) antibodies for 2 hours, followed by incubation with secondary rabbit-FITC and goat-Cy3 (1/300 dilution) antibody for 1 hour. 4',6-diamidino-2-phenylindole (DAPI) mounting medium (Vectashield, Vector Laboratories, Inc.,

Burlingame, CA, USA) was used to stain nuclei. Prepared slides were viewed under a Zeiss LSM 700 laser-scanning microscope (Carl Zeiss Microimaging GmbH) with the following conditions: Objective lenses, C-Apochromat 40x/1.20 W; Detectors, PMT; Filter model, DAPI (BP 420-475), Green (BP 490-555), and Red (560 IF); and Lasers, 405 nm, 488 nm, and 555 nm. Pictures were taken and analyzed using the ZEN2010 program (version 6.0.0.320).

2.10. MICROCOMPUTED TOMOGRAPHY (μCT)

Mouse calvariae were analyzed with a SkyScan 1172 scanner (SkyScan, Aartselaar, Belgium; 40 kV, 250 μA, 15 μm pixel size). Bone volumes were assessed by analyzing 5 mm regions between the occipital and the frontal calvarial bone with the CT-analyzer program. 3D images were obtained from the CT-volume program (version 1.11, SkyScan).

2.11. HISTOLOGY

Calvariae were fixed with 4% paraformaldehyde overnight and decalcified in 12% EDTA solution for 4 weeks. Decalcified samples were embedded in paraffin and sliced into 5 μm-thick sections with a Leica microtome

RM2145 (Leica Microsystems, Bannockbrun, IL, USA). The sections were baked at 50℃ for 30 minutes and paraffin was removed with xylene, followed by dehydration. The sections were then subjected to TRAP staining. Specimens were counterstained with hematoxylin.

2.12. NCBI GEO DATA BASE ANALYSES

Human S100A4 signal data were retrieved from GDS 2952, entitled **"**Expression profiling in RA disease pre and post anti-TNF treatment" (46, 47).

Human S100A4 signal data were retrieved from GSE 14020, entitled **"**Metastases of breast cancer" (30, 31).

2.13. ENZYME-LINKED IMMUNOSORBENT ASSAY (ELISA)

For mouse S100A4 ELISA, 4 X 10^4 BMMs/well were seeded into a 48-well tissue culture plate with 30 ng/ml M-CSF and 100 ng/ml RANKL. After the indicated day of culture, each well was filled with 100 μl serum free media further incubated for 24 hours, then subjected to ELISA following the manufacturer's protocol. For human S100A4 ELISA, 1/20-diluted synovial fluids of RA (n=15) and OA (n=15) patients were used. For human S100A4 ELISA of cancer cells,

10^5 cells/well were seeded into a 48-well tissue culture plate with DMEM. After overnight incubation, each well was replaced with 100 μl serum-free media and incubated for 24 hours. Supernatant was collected and then subjected to ELISA following the manufacturer's protocol.

2.14. PATIENTS SAMPLES

Synovial fluid samples were donated from 15 RA and 15 OA patients with permissions. Samples were stored at -80 ℃ and thawed before performing ELISA. Synovial fibroblast samples, donated from 63-year-old, 69-year-old and 75-year-old female RA patients, were collected and prepared as described previously (48). This study was approved by the Ethics Committee of Seoul National University Hospital.

2.15. TRANSCRIPTION FACTOR ELISAS

In order to measure the promoter binding activity, nucleus fractions of osteoclasts were prepared by using Nuclear Extract Kit from Active Motif (Carlsbad, CA), then 2 μg of the fractions were used to perform NF-κB family (p50, p52, p65 and RelB) or NFATc1 TransAM Transcription Factor ELISA

(Active Motif). The ELISAs were performed by following manufacturer's given protocol.

2.16. BrdU CELL PROLIFERATION ASSAY

BrdU cell proliferation assay kit was purchased from Calbiochem (Darmstadt, Germany). 10^4 cells were seeded into each well of 96-well plates. The rest of the assay was followed by manufacturer's protocol.

2.17. CELL MIGRATION ASSAY

Cell migration assay was done using 8.0 μm polycarbonate membrane Trans-well 24 well plates from Costar (Corning, NY). 3 x 10^4 cells were seeded onto upper chamber of the plate with serum-free DMEM while the lower chamber was filled with FBS-positive DMEM. After 12 hours of incubation, migrated cells were fixed with 3.7% fixing solution followed by crystal violet solution staining. Stained cells were dissolved with 10% acetic acid and subjected for ELISA reading at 595 nm.

2.18. CELL INVASION ASSAY

Cell invasion assay kit was purchased from Chemicon International (Billerica, MA). 3 x 10^5 cells were seeded onto upper chamber of the chamber provided in the kit. The rest of the procedure was followed by manufacturer's protocol.

2.19. CONDITIONED MEDIUM (CM) COLLECTION FROM CANCERS

10^6 cancer cells were seeded onto 60 mm tissue culture plate with DMEM media. Next day, media was exchanged to α-MEM and incubated for 24 hours. Then, the media was collected, followed by centrifugation for 5 minutes at 1200 rpm. The supernatant was collected and stored at -80℃ for future use.

2.20. cDNA MICROARRAY

Purified mRNAs from MCF7 and MDA-MB-231 were reverse-transcribed into cDNA and subjected to Human HT-12 Expression BeadChip kit (Illumina, CA), following manufacturer's protocol. The kit was designed to target more than 47,000 genes derived from the National Center for Biotechnology Information Reference Sequence.

2.21. STATISTICS

All experiments, except in vivo mice calvariae studies, were performed at least three times. Student's *t* test was used to define differences between two groups. Two-way ANOVA followed by the Bonferroni test was performed to define differences between multiple groups. $p < 0.05$ was considered significantly different.

CHAPTER 3

RESULTS

3.1. Effects OF S100A4 ON OSTEOBLAST

3.1.1. S100A4 DOES NOT AFFECT EARLY STAGE OF OSTEOBLAST DIFFERENTIATION

To test the effect of S100A4 on bone formation, I first investigated its influence on an in vitro culture of primary osteoblasts. Preosteoblasts derived from mouse calvarial tissues were treated with recombinant mouse S100A4 protein or control vehicle in osteogenic differentiation medium. Cells became positive for ALP, an early stage marker of osteoblast differentiation, within 3 days of culture in osteogenic media (Figure 4). S100A4 treatment did not alter the extent of ALP staining compared to the vehicle-treated culture (Figure 4). Consistently, I did not observe any differences in ALP activity by S100A4 treatment at day 2 or day 4 of the culture (Figure 5). I next assessed mRNA and protein levels of Runx2, the key transcription factor of early osteoblast differentiation. The mRNA expression of Runx2 in S100A4-treated cultures was comparable to that in the vehicle-treated group (Figure 6). On the other hand, I observed a slight decrease in Runx2 protein level by S100A4 treatment at day 3 of the culture (Figure 7). Taken together, these results indicate that S100A4 has little effect on the early stage of osteoblast differentiation.

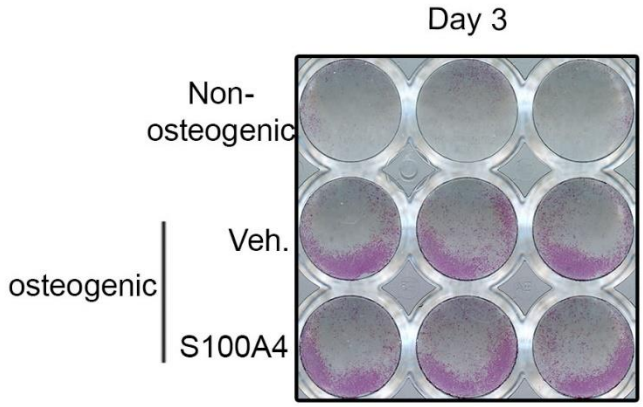

Figure 4. S100A4 treatment did not change the extent of ALP staining compared to the vehicle-treated culture.

Mouse calvarial osteoblasts cultured with non-osteogenic or osteogenic medium containing vehicle (Veh.) or recombinant mouse S100A4 protein (1 μg/ml) were ALP-stained after 3 days of culture.

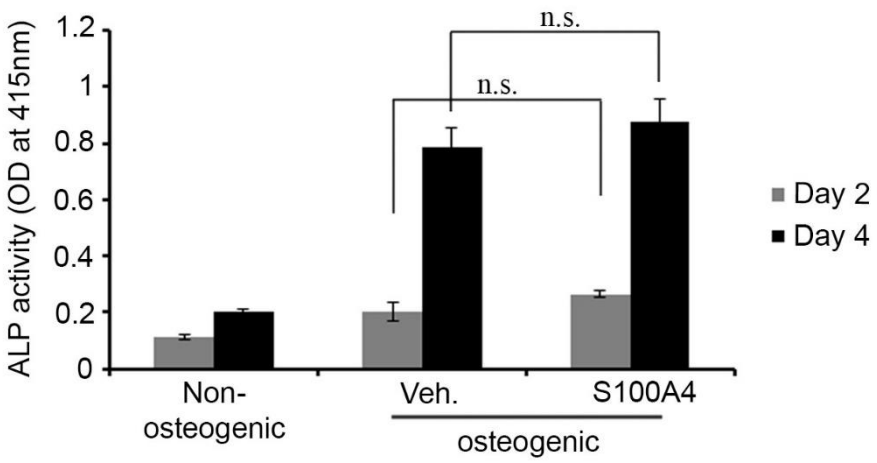

Figure 5. S100A4 treatment did not change the extent of ALP activity compared to the vehicle-treated culture.

Mouse calvarial osteoblasts cultured with non-osteogenic or osteogenic medium containing vehicle (Veh.) or recombinant mouse S100A4 protein (1 μg/ml) were subjected for ALP activity measurement at day 2 and day 4.

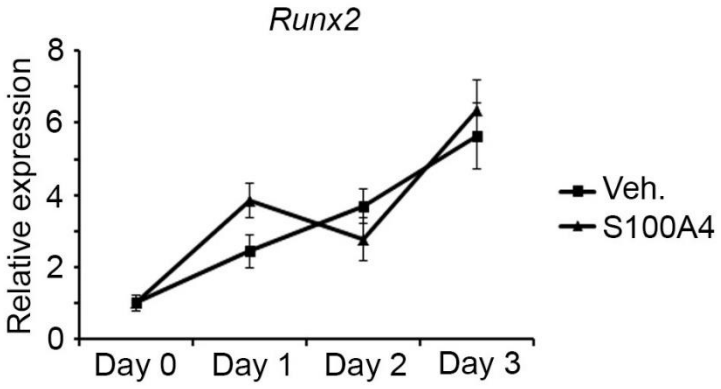

Figure 6. The mRNA expression of Runx2 in S100A4-treated cultures was comparable to that in the vehicle-treated group.

Mouse calvarial osteoblasts were cultured with vehicle or recombinant mouse S100A4 protein in osteogenic medium for the indicated days and subjected to real-time PCR for *Runx2* expression. HPRT was used as an internal control.

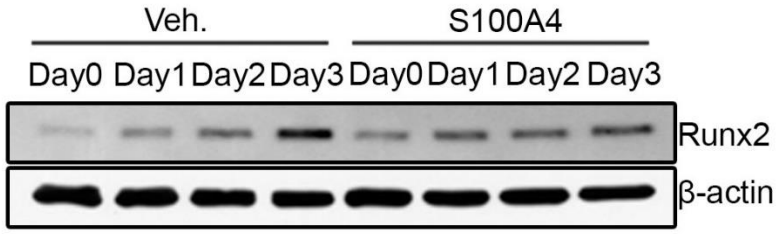

Figure 7. A slight decrease in Runx2 protein levels by S100A4 treatment at day 3 of the culture was observed.

The protein levels of Runx2 were assessed by Western blotting. β-Actin is shown as a loading control.

3.1.2. S100A4 INHIBITS MINERALIZATION AND THE EXPRESSION OF LATE-STAGE OSTEOBLAST MARKERS

I assessed the effect of S100A4 on matrix mineralization, a crucial function of osteoblast during bone formation. Interestingly, the addition of S100A4 in osteogenic media significantly delayed matrix mineralization by calvarial osteoblasts at day 10, as shown by Alizarin-red staining (Figures 8A and B). The expression level of osteocalcin (*Bglap*), a critical component of bone matrix, was also decreased by S100A4 treatment (Figure 9). Induction of the protein level of osterix, a transcription factor necessary for mineralization, was also suppressed by S100A4 treatment (Figure 10). Collectively, these results show that an excessive amount of extracellular S100A4 impairs the mineralization activity of osteoblasts and delays induction of late osteoblast markers.

A

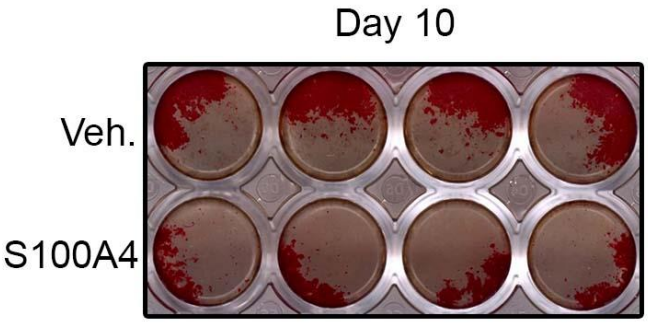

B

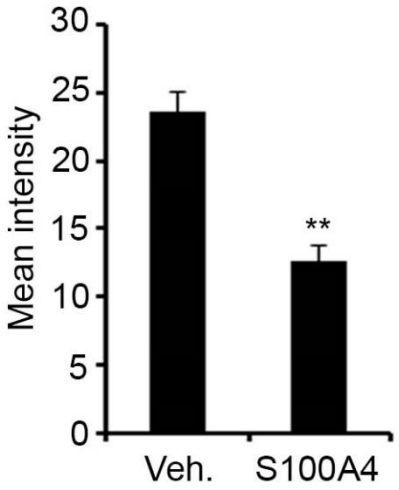

Figure 8. The addition of S100A4 in osteogenic media significantly delayed matrix mineralization by calvarial osteoblasts at day 10.

(A) Mouse calvarial osteoblasts were cultured with vehicle or recombinant mouse S100A4 protein in osteogenic medium for 10 days. Alizarin-red staining was performed and a representative image is shown. (B) The intensity of the image from (A) was measured using ImageJ and is depicted in a graph.

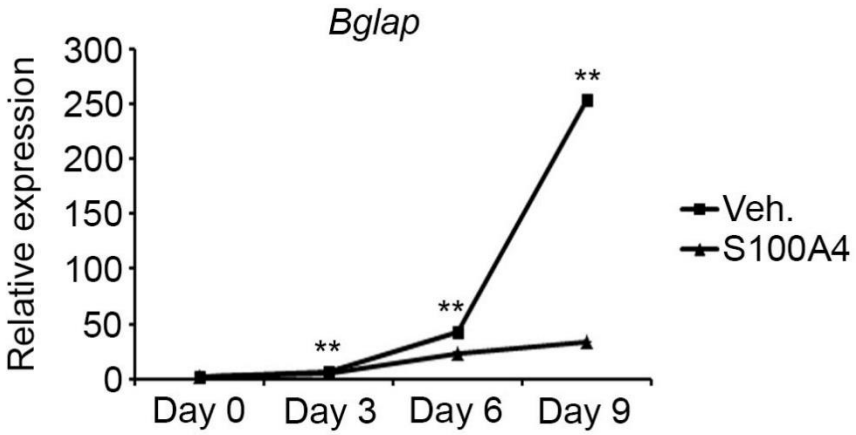

Figure 9. The expression level of osteocalcin was decreased by S100A4 treatment.

Mouse calvarial osteoblasts were cultured with vehicle or recombinant mouse S100A4 protein in osteogenic medium for the indicated days and subjected to real-time PCR for *Bglap* (osteocalcin) expression. HPRT was used as an internal control.

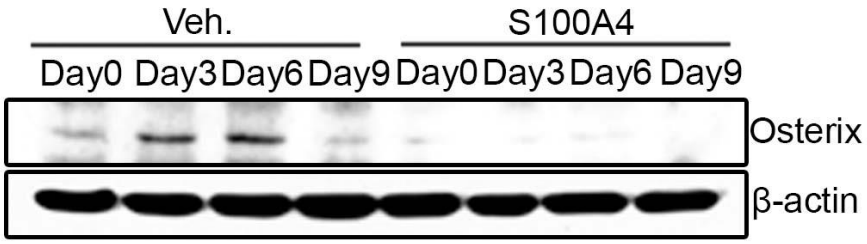

Figure 10. The induction of protein levels of osterix was suppressed by S100A4 treatement.

Mouse calvarial osteoblasts were cultured with vehicle or recombinant mouse S100A4 protein in osteogenic medium for the indicated days. The protein levels of osterix were assessed by Western blotting. β-Actin was included as a loading control.

3.1.3. S100A4 ACTIVATES THE NF-κB PATHWAY

A number of studies have reported that activation of the NF-κB pathway in osteoblast precursors impaired osteogenic differentiation (37, 38). To investigate the mechanism of mineralization inhibition by S100A4, I tested whether S100A4 activated the NF-κB pathway in calvarial osteoblasts. I stimulated calvarial osteoblasts with recombinant mouse S100A4 and observed the phosphorylation of IKKα/β, IκB, and p65 within 60 minutes (Figure 11). I also assessed the protein level of p65 in the nucleus by fractionating the cytosol and nuclear proteins. Increased levels of p65 were observed in the nuclei of S100A4-treated cells (Figure 12). Consistent with our Western blotting results, immunofluorescence confocal microscopy also demonstrated localization of p65 in the nuclei after S100A4 stimulation (Figure 13). These data suggest that S100A4 negatively regulates osteogenic differentiation by activating the NF-κB signaling pathway.

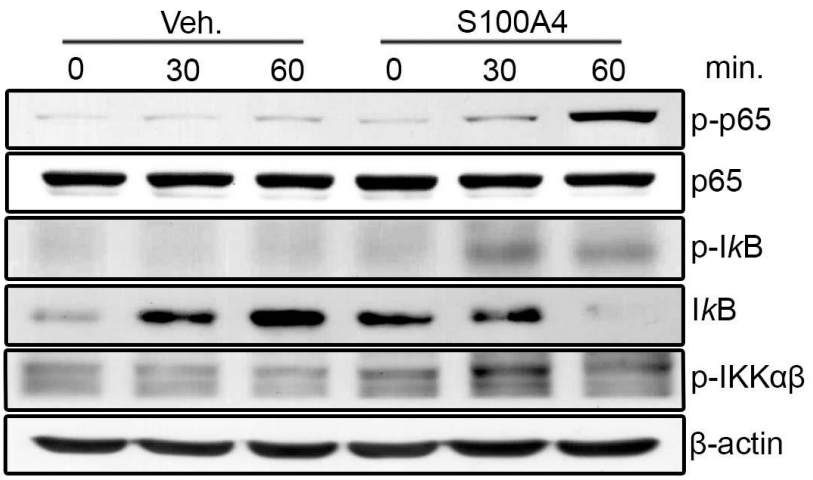

Figure 11. S100A4 activated the NF-κB pathway in osteoblasts.

Mouse calvarial osteoblasts were serum-starved for 5 hours, stimulated with either vehicle or recombinant mouse S100A4 (2 μg/ml) for the indicated time, and subjected to Western blotting to detect protein levels of phosphorylated p65 (p-p65), total p65, phosphorylated IκB (p-IκB), total IκB and phosphorylated IKKαβ. β-Actin is shown as a loading control.

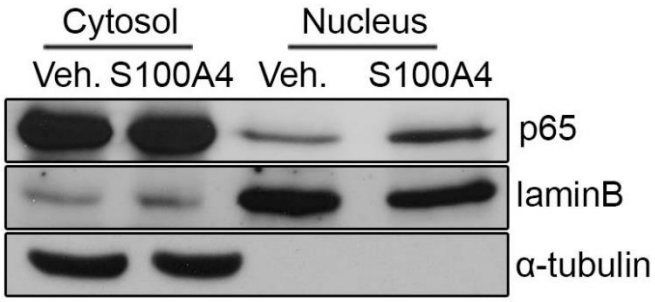

Figure 12. Increased levels of p65 were observed in the nuclei of S100A4-treated osteoblasts.

Mouse calvarial osteoblasts were serum-starved for 5 hours and stimulated with either vehicle or recombinant mouse S100A4 (2 μg/ml) for 1 hour. Cytosolic proteins (30 μg) and nuclear proteins (8 μg) were separated and subjected to Western blotting to detect protein levels of p65, laminB, and α-tubulin.

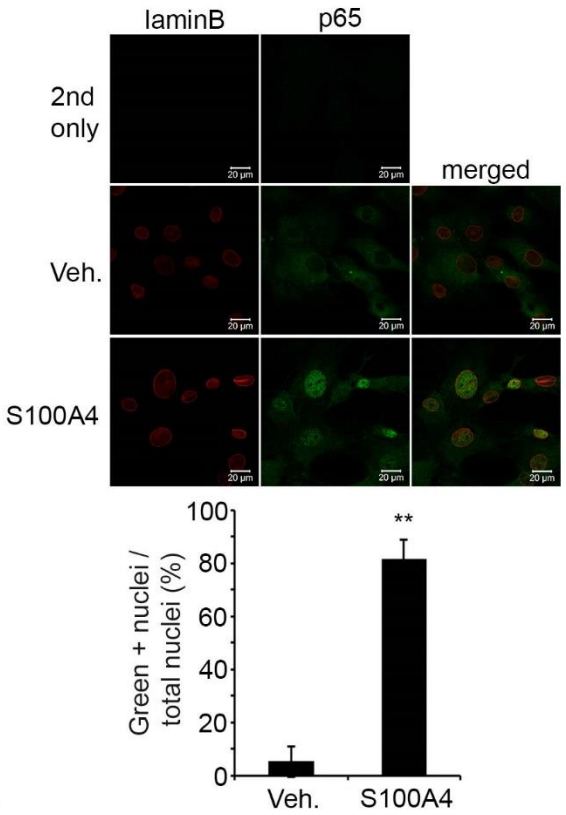

Figure 13. Increased localization of p65 in the nuclei of S100A4-treated osteoblasts was observed.

Mouse calvarial osteoblasts were serum-starved for 5 hours and stimulated with either vehicle or recombinant mouse S100A4 (2 μg/ml) for 1 hour. Cells were stained with anti-laminB (red) and anti-p65 (green). LaminB was labeled to locate the nuclear membrane. Cells were subjected to confocal microscopy and representative images are shown (upper). Green positive (+) nuclei were counted and are depicted as a graph (lower). Primary antibodies were not added for 2nd only samples.

3.1.4. S100A4 INTERFERES WITH MINERAL APPOSITION IN VIVO DURING CALVARIAL BONE FORMATION

To study the effect of S100A4 on bone formation in vivo, I subcutaneously injected recombinant mouse S100A4 protein onto 1-day-old mice calvariae, where precursors of osteoblasts are abundantly present. Calcein was intraperitoneally injected twice with a 4-day interval to measure mineral apposition rates (Figure 14). The first calcein injection marked the mineral level at the initial point, while the second injection marked newly formed minerals. The distance between the two calcein-marked lines reflects the quantity of minerals deposited during the injection period; the distance (i.e., the quantity) was decreased by S100A4 treatment (Figure 15A). Calculation of the mineral apposition rate revealed a significantly reduced rate in the S100A4-injected group (Figure 15B).

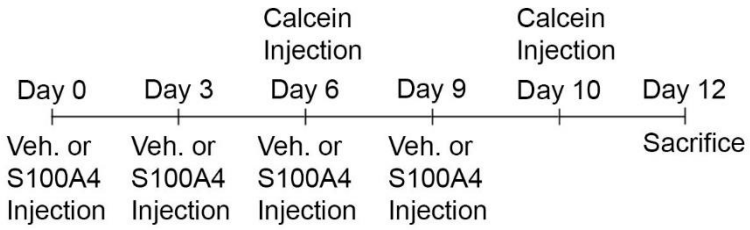

Figure 14. A schematic timeline describing the experiment.

Mouse recombinant S100A4 (5 μg) or vehicle was injected onto neonatal mouse calvariae starting from day 0 with 3 days of intervals for total of 4 injections. Intraperitoneal calcein (25 mg/kg) injections were performed on days 6 and 10. Mice were sacrificed at day 12; n=7 for each test group.

A

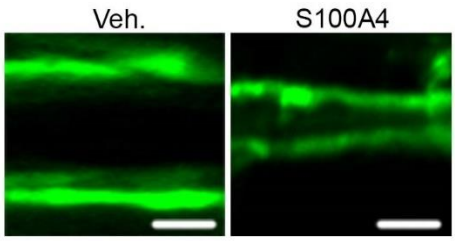

B

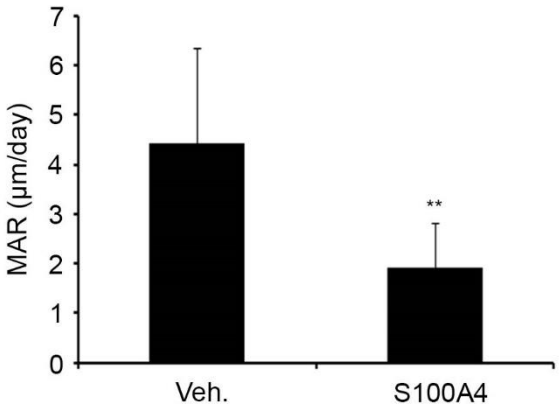

Figure 15. S100A4 disrupts with the mineral apposition in vivo during calvarial bone formation.

(A) Representative images of calcein labeled calvarial tissue sections are shown. (B) Daily mineral apposition rates were calculated by measuring distances between two calcein labeled lines. Randomly chosen images from each test group were analyzed. **, $p < 0.01$ values compared between S100A4 and vehicle. Scale bar represents 10 μm. MAR, mineral apposition rate

3.2. ROLE OF S100A4 IN OSTEOCLASTOGENESIS

3.2.1. HIGH EXPRESSION OF S100A4 IN RHEUMATOID ARTHRITIS

In an effort to find genes differentially expressed in specimens from RA patients, I analyzed cDNA microarray data deposited in NCBI GEO. The analysis of the expression profiling of whole blood samples from RA patients followed by anti-TNF treatment [GDS2952] revealed that S100A4 expression was higher in RA patients in comparison with normal individuals, while the post-treated group still maintained increased levels of S100A4 (Figure 16). To confirm the elevated expression of S100A4 in RA patients, I assessed S100A4 protein concentrations in synovial fluid samples from RA and OA patients by ELISA. As shown in Figure 17, S100A4 levels were significantly higher in RA patients than in OA patients (Figure 17). These results are consistent with previous reports that showed increased S100A4 expression in synovial fibroblasts and synovial tissues from RA patients (31).

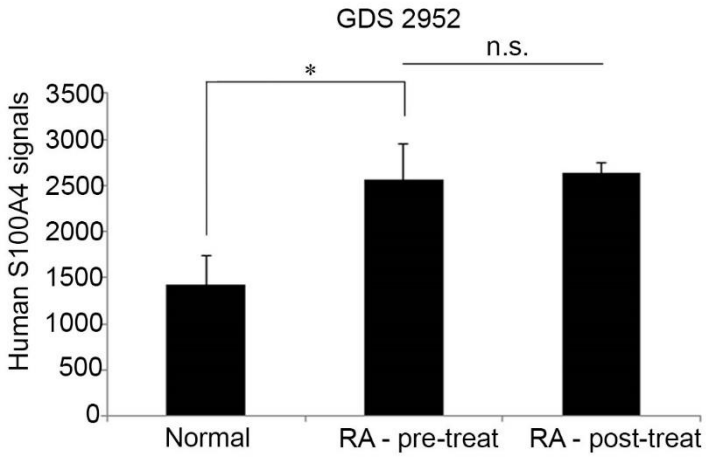

Figure 16. Elevated expression of S100A4 in RA patients was retrieved from GDS 2952.

Human S100A4 signals of RA patients, Enbrel-treated RA patients, and normal individuals were analyzed with GDS 2952 data set in GEO data base.

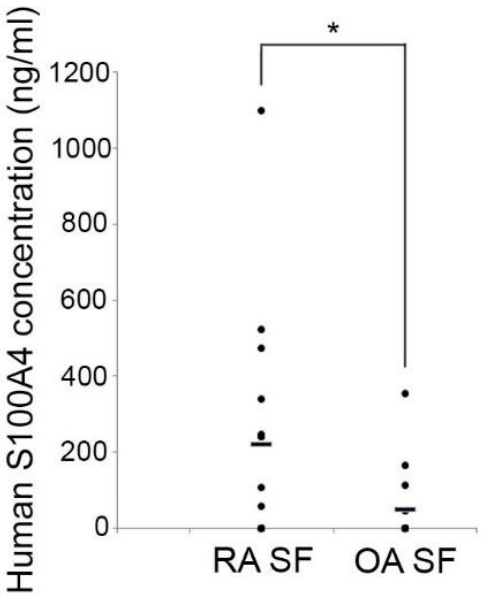

Figure 17. High concentrations of S100A4 were observed in synovial fluid of RA patients.

S100A4 protein levels were measured in synovial fluid (SF) samples of RA (n = 15) and osteoarthritis (OA) patients (n = 15) by human S100A4 ELISA.

3.2.2. S100A4 REDUCES BONE VOLUME

As RA conditions involve osteoclastic bone erosion and secretory molecules up-regulated in RA synovium may modulate osteoclast activity, I next tested whether S100A4 could stimulate bone resorption by osteoclasts. BMMs treated with S100A4 were cultured with M-CSF and RANKL on dentine slices. RANKL-induced osteoclasts with the addition of S100A4 significantly resorbed dentin slices wider and deeper compared to the vehicle control (Figure 18). I also investigated the effect of S100A4 on bone in vivo by injecting recombinant mouse S100A4 protein (10 μg/mouse) subcutaneously onto mouse calvariae. 3D-reconstituted images created by μCT analysis indicated that the S100A4 injection did cause decreased bone volume (Figure 19).

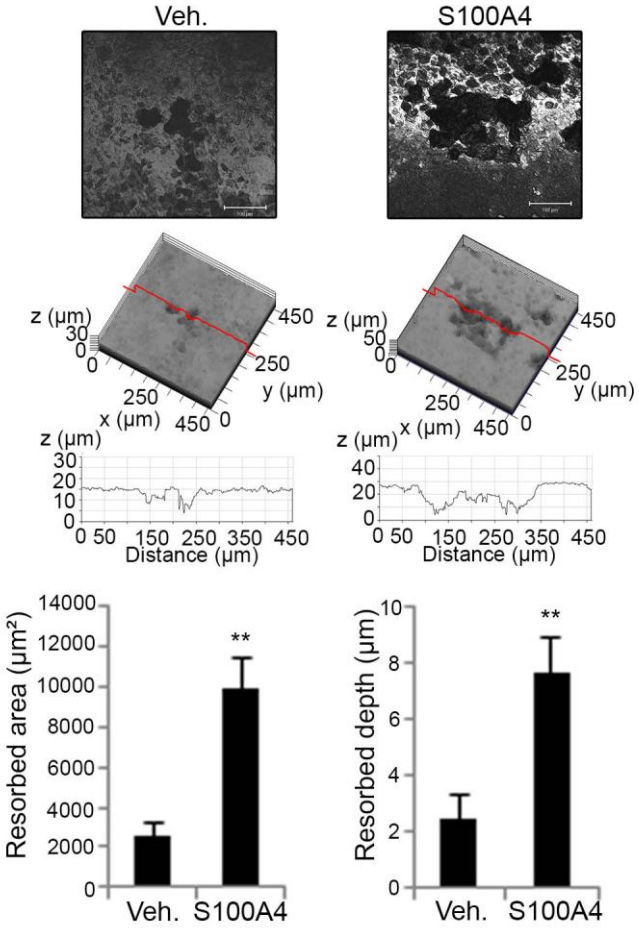

Figure 18. Bone resorbing activity of osteoclast was enhanced by S100A4.

BMMs treated with S100A4 or vehicle were cultured with M-CSF and RANKL on dentine slices. Dentine slices were analyzed by confocal laser microscopy. Representative images of each sample from a region on a dentine slice were shown (upper). Resorbed area and depth were calculated and depicted as graphs (lower).

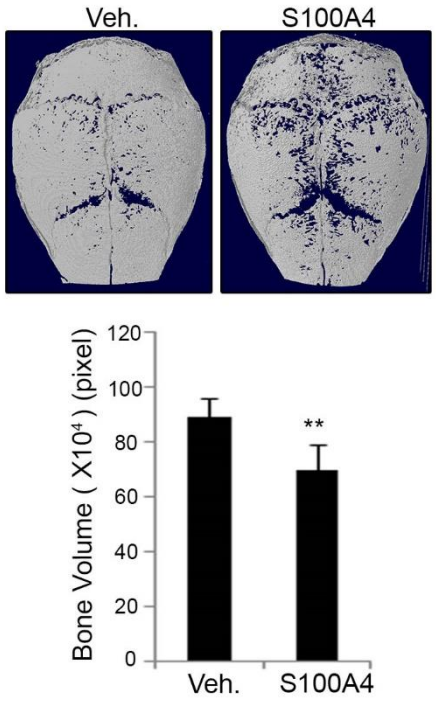

Figure 19. S100A4 injection decreased bone volume of mouse calvariae.

Recombinant mouse S100A4 proteins or vehicle were subcutaneously injected onto mouse calvariae every other day for 8 days and sacrificed. 3D images were created after micro-CT analysis (upper) and bone volumes were analyzed (lower).

3.2.3. S100A4 ENHANCES OSTEOCLAST DIFFERENTIATION

Given the increase in bone resorption by S100A4 seen in Figure 18 and 19, I examined whether S100A4 would directly induce osteoclast differentiation. First of all, BMMs with different concentrations of recombinant S100A4 were differentiated into osteoclasts with RANKL and I observed dose-dependent inhibition of osteoclastogenesis (data not shown). However, when pre-fusion osteoclasts (pOCs), 2-day RANKL-primed BMMs, were driven to differentiate into mature osteoclasts by RANKL in the presence of variable concentrations of recombinant mouse S100A4, dose-dependent increase of osteoclast differentiation was observed (Figure 20). Next, the effect of S100A4 on osteoclastogenesis was studied in the in vivo calvarial injection experiments. The calvaira sections were TRAP stained to visualize osteoclasts and quantification of osteoclasts were followed. As a result, the percentages of osteoclast surfaces over bone surfaces were dramatically increased in the S100A4-injected group (Figure 21). Furthermore, in vitro stimulation of pOCs with S100A4 dramatically increased mRNA expressions of osteoclast differentiation markers such as *Ctsk*, *Dcstamp* and *Mmp9*. (Figure 22). I also confirmed by Western blotting that a total protein level of NFATc1, a master transcription factor in osteoclast, increased prominently in S100A4 stimulated pOCs (data not shown). Furthermore, I isolated a nucleus fraction of S100A4-stimulated pOCs and the fractions were subjected to

transcription factor ELISA. As a result, I observed a stronger promoter binding of NFATc1 in S100A4-treated fraction (Figure 23).

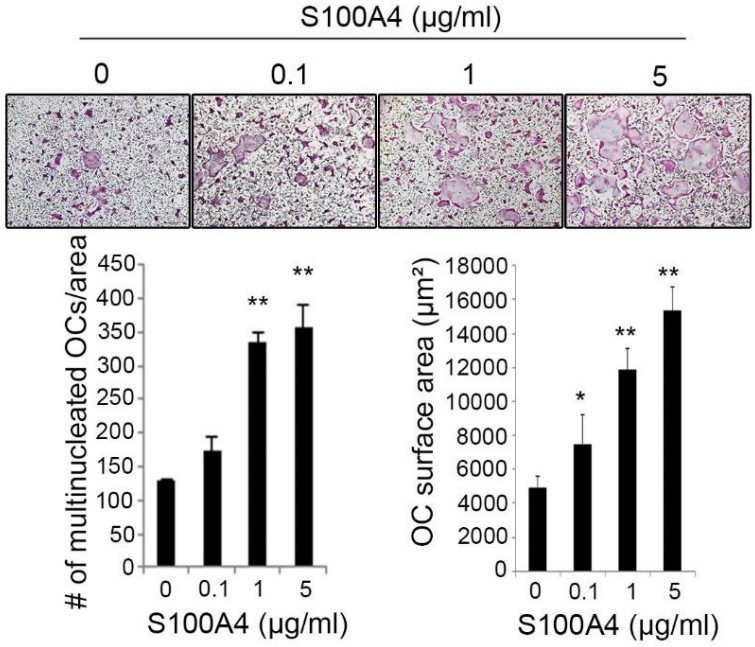

Figure 20. S100A4 increased osteoclast differentiation.

BMMs were committed to osteoclasts with RANKL for 2 days, then treated with various concentrations of recombinant mouse S100A4 proteins and stained for TRAP activity.

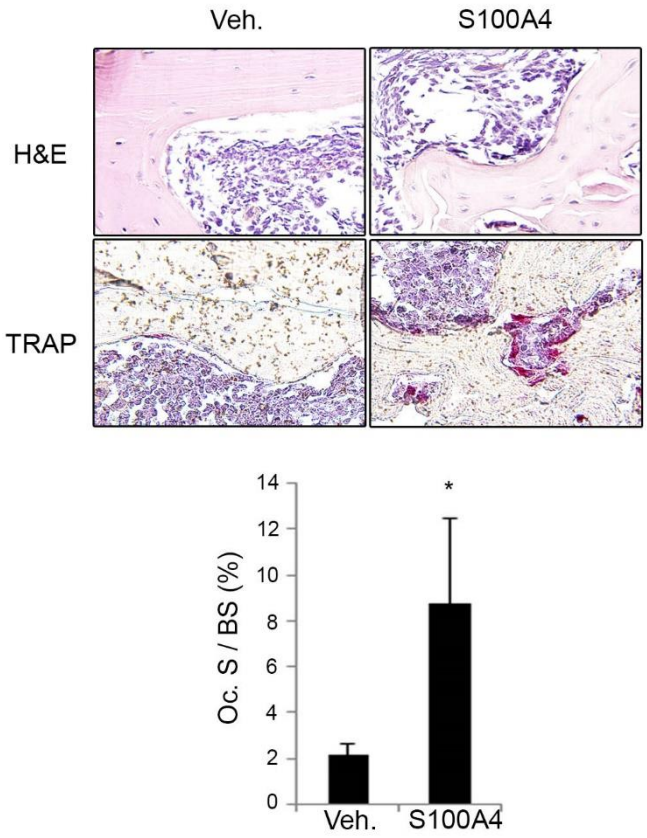

Figure 21. Elevated numbers of osteoclasts were observed in S100A4-injected mouse calvariae.

Mice calvaria analyzed in Fig. 5D were subjected to paraffin sectioning. Calvariae tissue sections were stained for TRAP (upper). Osteoclast surface over total bone surface (Oc.S/BS) (%) was determined (lower).

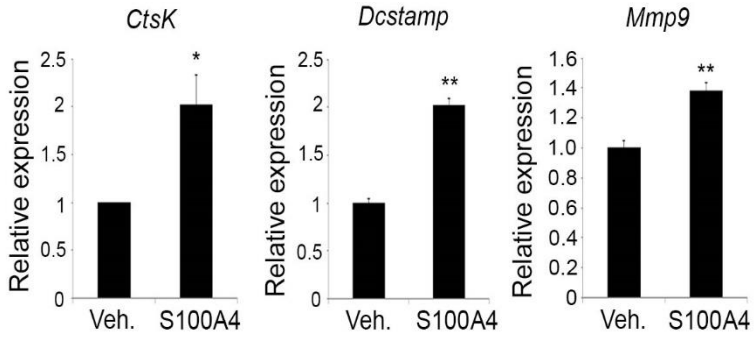

Figure 22. Osteoclast marker genes were up-regulated by S100A4 treatment.

BMMs were committed to osteoclasts with RANKL for 2 days, then pOCs were treated with recombinant mouse S100A4 proteins (1 μg/ml) or vehicle for a day. The mRNA levels of *CtsK, Dcstamp, and Mmp9* were analyzed by real-time PCR.

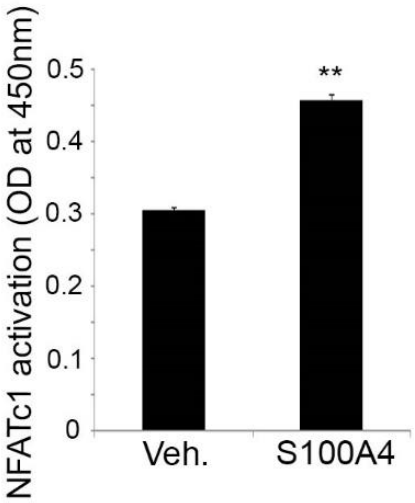

Figure 23. NFATc1 activation was observed after S100A4 treatment in osteoclasts.

After stimulation with S100A4 (1 μg/ml) or vehicle, nucleus fractions of pOCs were used to measure the NFATc1 activation by the transcription factor ELISA.

3.2.4. ACTIVIATION OF MAPK AND NF-κB PATHWAY BY S100A4 IN OSTEOCLASTS

Since RANKL-induced osteoclastogenesis involves activation of MAPK and NF-κB pathway, I next tested whether S100A4 solely mediates such activations (4-7, 49). pOCs were serum starved for 4 hours and stimulated with S100A4. Surprisingly, MAPK and NF-κB signals were activated by S100A4 stimulation, as shown by phosphorylations of extracellular signal-regulated kinase (ERK), c-Jun N-terminal kinase (JNK), p38, IKKαβ, IκB and p65 (Figure 24). Moreover, immunofluorescence confocal microscopy demonstrated localization of p65 in the nuclei after S100A4 stimulation (Figure 25). In order to find which NF-κB pathways, the canonical or the non-canonical, might be activated upon S100A4 treatment in osteoclasts, I isolated the nuclear proteins of vehicle or S100A4 treated pOCs to perform the NF-κB family transcription factor ELISA. Interestingly, only p65 and p50, transcription factors critical in the canonical NF-κB pathway, were activated by S100A4, whereas no difference was observed in the activation of RelB and p52 which are known to be involved in the non-canonical NF-κB pathway (Figure 26).

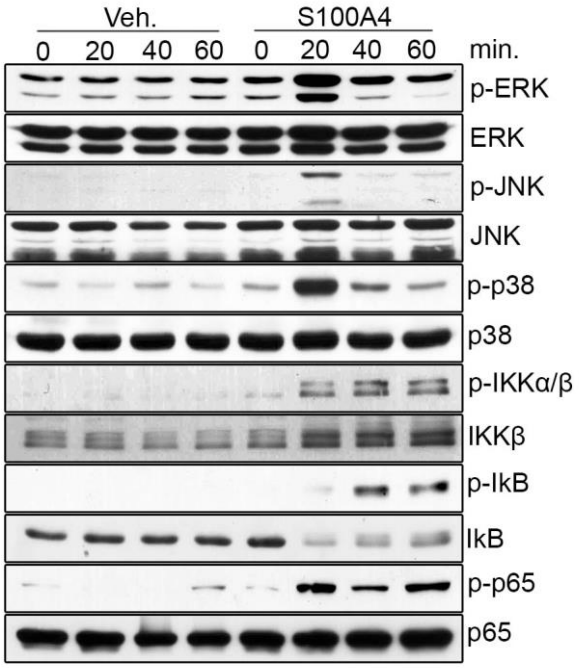

Figure 24. S100A4 activated MAPK and NF-κB pathways in osteoclasts.

pOCs were serum-starved for 5 hours and stimulated with either vehicle or recombinant mouse S100A4 (2 μg/ml) for the indicated time and subjected to Western blotting to detect protein levels of phosphorylated ERK (p-ERK), total ERK, phosphorylated JNK (p-JNK), total JNK, phosphorylated p38 (p-p38), total p38, phosphorylated p65 (p-p65), total p65, phosphorylated IκB (p-IκB), total IκB, phosphorylated IKKαβ (p-IKKαβ), and total IKKβ.

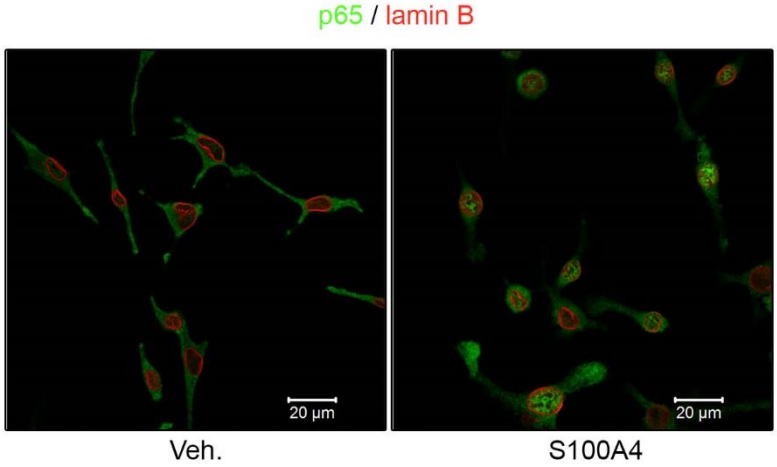

Figure 25. Increased nuclei localization of p65 was observed after S100A4 stimulation in osteoclasts.

pOCs were serum-starved for 5 hours and stimulated with either vehicle or recombinant mouse S100A4 (1 μg/ml) for an hour. Cells were stained with anti-laminB (red) and anti-p65 (green). LaminB was labeled to locate the nuclear membrane. Cells were subjected to confocal microscopy and representative images are shown.

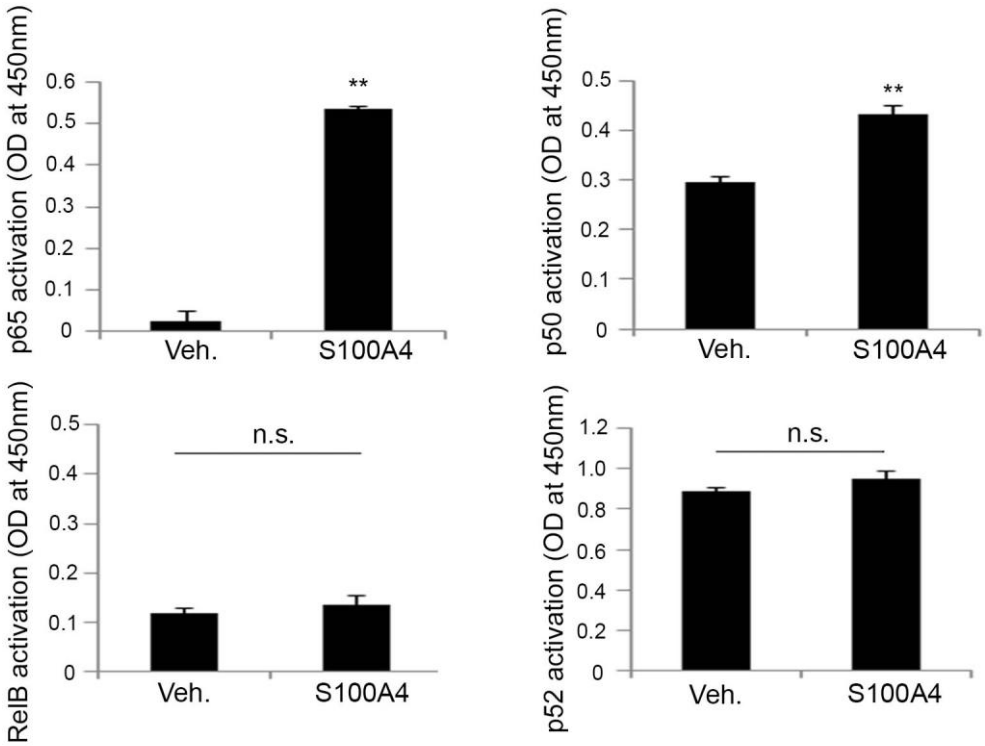

Figure 26. S100A4 activated the canonical NF-κB pathway rather than the non-canonical NF-κB pathway in osteoclasts.

Activations of p65, p50, RelB, and p52 in pOCs were measured by NF-κB family transcription factor ELISA after S100A4 (1 μg/ml) or vehicle treatment for an hour.

3.2.5. REDUCTION OF S100A4-STIMULATED OSTEOCLASTOGENESIS BY DOWN-REGULATING RAGE

Increasing evidence supports that S100 proteins interact with RAGE to mediate down-stream signals such as the NF-κB pathway (40). Given that, I investigated to assure that RANKL-induced osteoclasts do express RAGE to mediate S100A4 down-stream signals observed in the previous figures. As demonstrated by Western blotting, the protein levels of RAGE increased by RANKL stimulation and remained high until maturation of the osteoclasts (Figure 27). To investigate the role of RAGE in S100A4-stimulated osteoclastogenesis, I down-regulated the expression of RAGE by si-RNA. Successful down-regulation was confirmed by RT-PCR and Western blotting (Figure 28 upper). Next, I tested if the RAGE down-regulated BMMs with S100A4 stimulation would form osteoclasts normally. Indeed, the number of TRAP-positive osteoclasts and their surface areas were greatly reduced by RAGE down-regulation, even with the S100A4 stimulus at the concentration that enhances osteoclastogenesis (Figure 28 lower). As mentioned earlier, RAGE mediates the NF-κB signaling pathway and I described the activation of NF-κB signals by S100A4 in figure 24. Thus, I was interested in examining whether RAGE down-regulated osteoclasts would retain the activation of NF-κB signaling in response to S100A4 stimulation. As expected, phosphorylation of p65 and IκB was reduced more in the RAGE down-

regulated osteoclasts than the control (Figure 29). Finally, the increase in expression of osteoclast markers by S100A4 stimulation was also down-regulated significantly after the RAGE knock-down. (Figure 30).

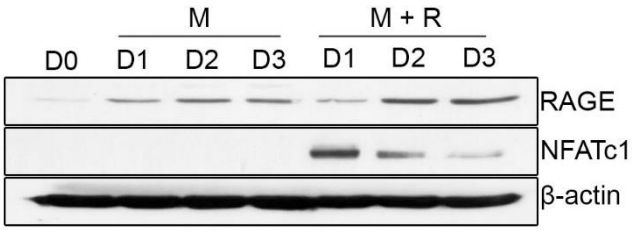

Figure 27. RAGE expression was increased by RANKL.

BMMs were cultured with M-CSF (M) or M-CSF and RANKL (M+R) for the indicated days. The protein levels of RAGE and NFATc1 were assessed by Western blotting. β-Actin was included as a loading control.

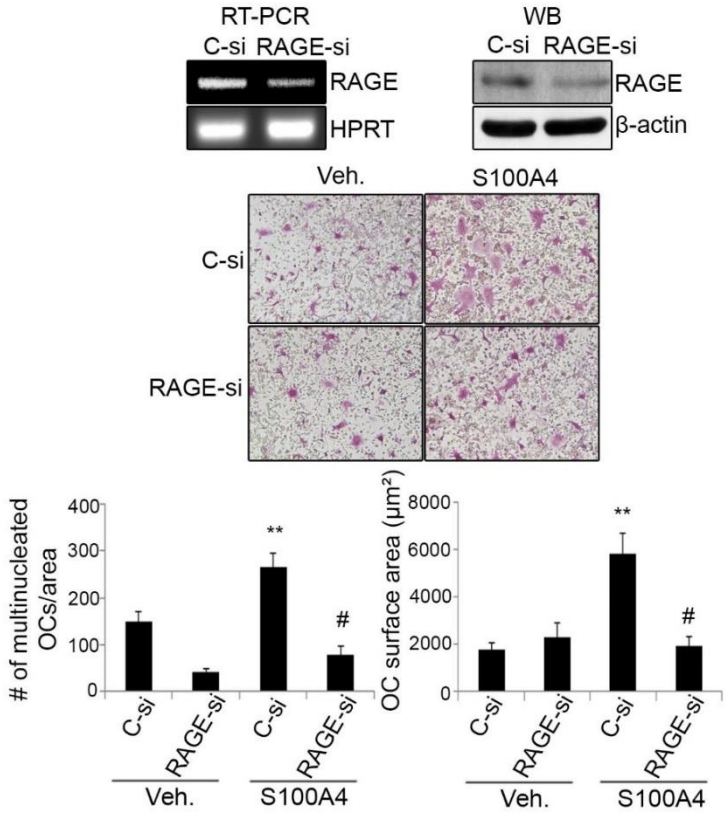

Figure 28. Down-regulation of RAGE prevented increased osteoclast differentiation by S100A4.

BMMs were transfected with control siRNA (C-si) or RAGE-targeted siRNA (RAGE-si). The expression of RAGE was assessed by RT-PCR and Western blot analysis (upper). Transfected BMMs cultured with M-CSF and RANKL were TRAP-stained and counted for 3 or more nuclei. Osteoclast (OC) surface area was also measured (lower). **, versus vehicle-treated C-si sample; #, significantly different versus S100A4-treated C-si sample.

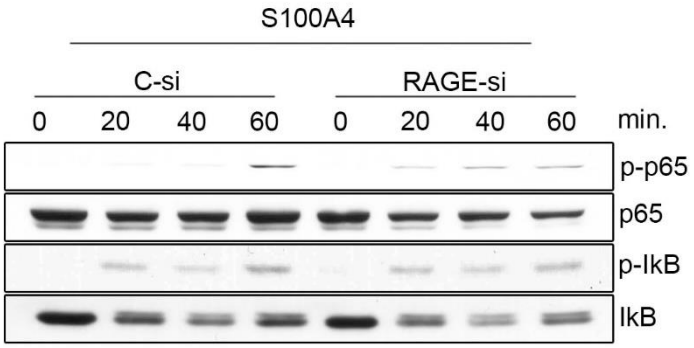

Figure 29. Down-regulation of RAGE decreased the NF-κB activation caused by S100A4.

BMMs were transfected with control siRNA (C-si) or RAGE-targeted siRNA (RAGE-si). Transfected BMMs were serum-starved for 4 hours followed by S100A4 stimulation for the indicated time. Whole cell lysates were subjected to Western blot analyses to detect p-p65, p65, p-IκB, and IκB.

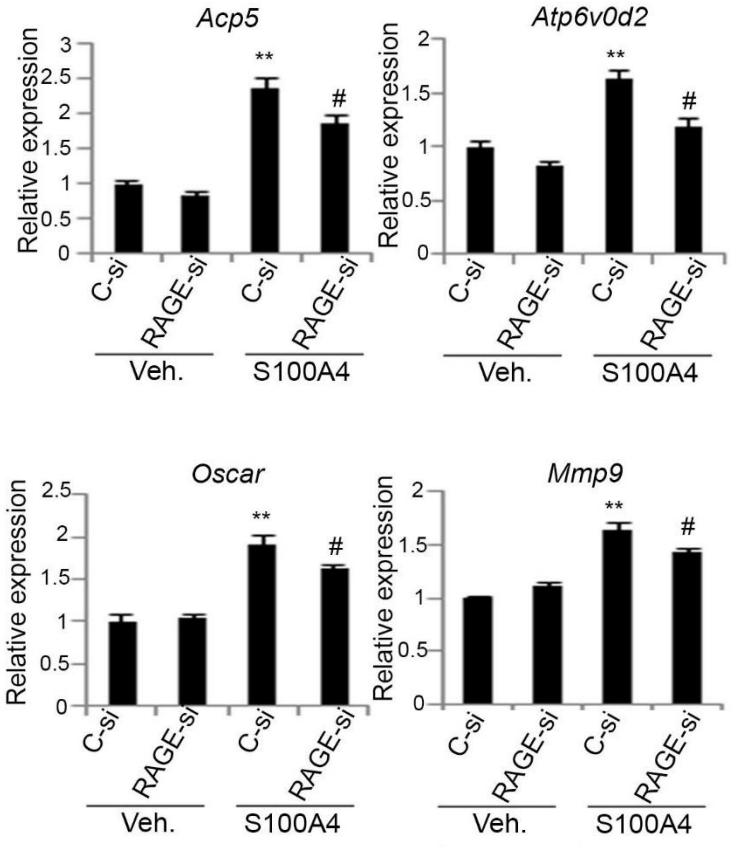

Figure 30. Down-regulation of RAGE decreased the expression of osteoclast marker genes that were elevated by S100A4 treatment.

BMMs transfected with C-si or RAGE-si were cultured with M-CSF and RANKL for 2 days, then cultured with vehicle or S100A4 for a day. Real-time PCR was performed to examine expression of *Acp5*, *Atp6v0d2*, *Oscar*, *and Mmp9.* **, versus vehicle-treated C-si sample; #, significantly different versus S100A4-treated C-si sample.

3.2.6. SECRETION OF S100A4 FROM OSTEOCLASTS AND ITS NECESSITY IN RANKL-INDUCED OSTEOCLASTOGENESIS

Series of studies reported that activated macrophages and tumors express and secrete S100A4 upon certain stimulations (50-52). Therefore, I assessed if BMMs express and secrete S100A4 by RANKL stimulation. Indeed, the expression of S100A4 clearly increased by RANKL stimulation in the presence of M-CSF (Figure 31). Not only did the mRNA level of S100A4 increase, but the protein levels of S100A4 in whole cell lysates also increased, (data not shown) while media secretion augmented even more dramatically by RANKL stimulation (Figure 32 upper). This again was confirmed by mouse S100A4 ELISA (Figure 32 lower). Next, I examined the down-stream signaling pathway of RANKL that mediated secretion of S100A4. Thus, I treated pharmaceutical inhibitors, SB203580, LY294002, SP600125 and Bay11-7085, to block the activation of p38, PI3K, JNK and NF-κB respectively. Interestingly, all of the inhibitors decreased S100A4 secretion from osteoclasts (Figure 33). Notably, secretion of S100A4 was completely abolished by Bay11-7085 treatment, indicating NF-κB as a key component of S100A4 secretion during osteoclastogenesis. Based on what I have observed, I speculated that the secreted S100A4 could enhance osteoclastogenesis in an autocrine manner. Thereby, I added S100A4 neutralizing antibodies to block the secreted S100A4 during RANKL-induced osteoclast differentiation. As shown

in Figure 34, a great reduction in the number of TRAP-positive osteoclasts and the areas were observed in an antibody dose-dependent manner, demonstrating the role of secreted-S100A4 during osteoclastogenesis (Figure 34).

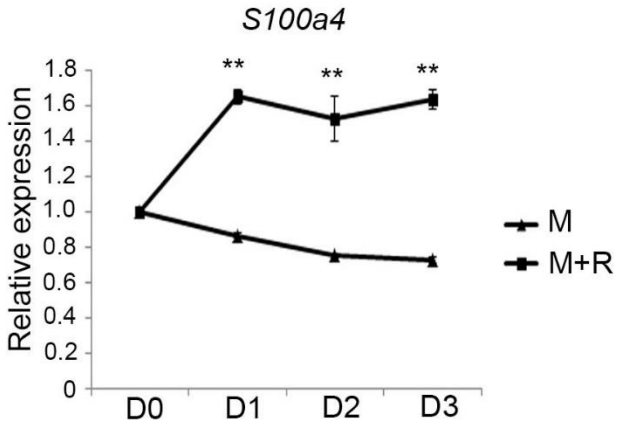

Figure 31. RANKL increased the S100A4 expression during osteoclast differentiation.

BMMs were cultured with M or M+R for the indicated days and subjected to real-time PCR for *S100a4* expression. HPRT was used as an internal control. M, M-CSF; R, RANKL.

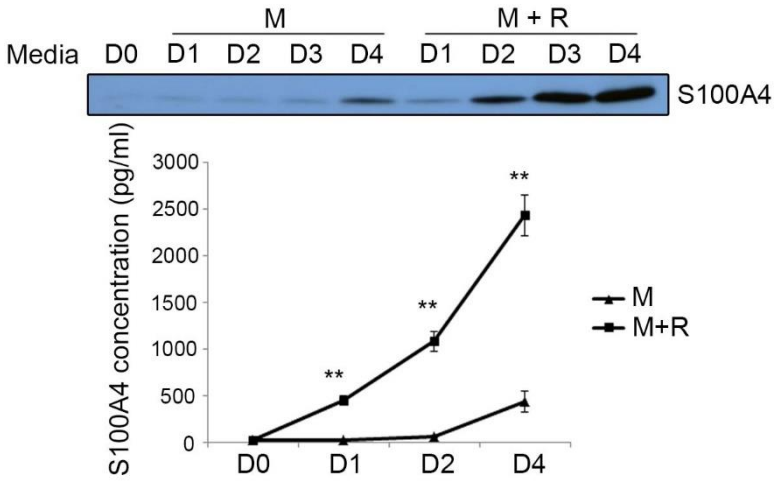

Figure 32. RANKL increased secretion of S100A4 during osteoclast differentiation.

BMMs were cultured with M or M+R for the indicated days and culture supernatant was subjected for Western blot (upper) analysis and mouse S100A4 ELISA (lower) to measure secreted S100A4. M, M-CSF; R, RANKL.

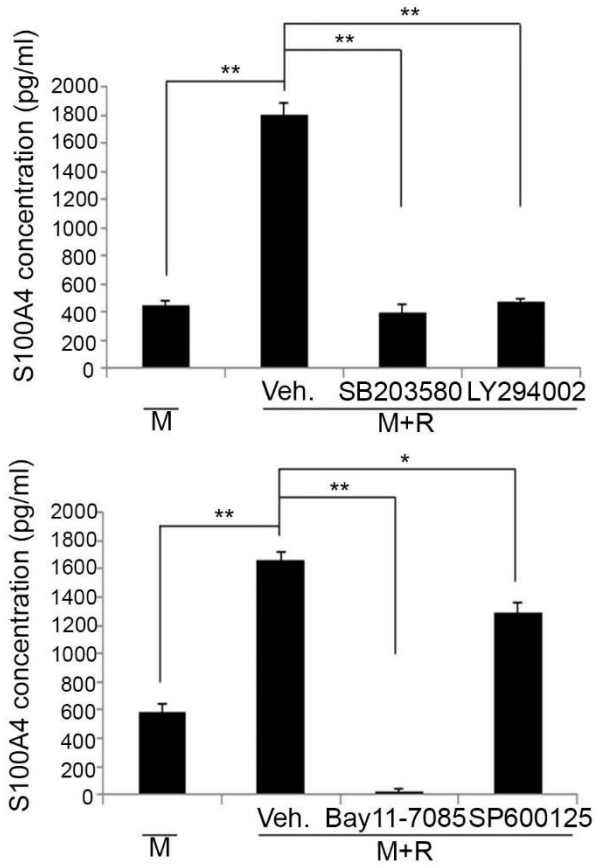

Figure 33. S100A4 secretion was abrogated by inhibiting crucial signaling pathways regulated by RANKL.

SB203580 (10 μM), LY294002 (10 μM), Bay11-7085 (10 μM) and SP600125 (10 μM) or DMSO were added to BMMs during RANKL-induced osteoclastogenesis. 5 days after initial treatments, culutre supernatant was collected and subjected to mouse S100A4 ELISA. M indicates M-CSF (30 ng/ml)

only treated samples and M+R indicates M-CSF (30 ng/ml) and RANKL (100 ng/ml) treated samples. M, M-CSF; R, RANKL

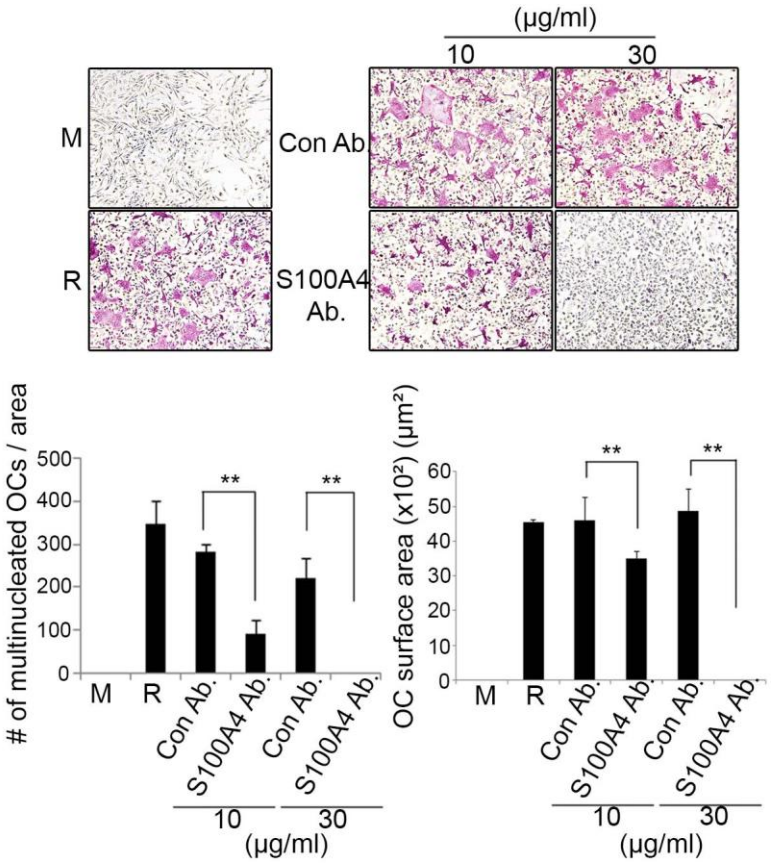

Figure 34. Neutralization of S100A4 abrogated osteoclast differentiation.

BMMs cultured with M or M+R were treated with control or S100A4 neutralizing antibody at the indicated concentration and TRAP stained. Representative images were shown (upper). TRAP-positive cells with 3 or more nuclei were counted (lower left) and OC surface area was measured (lower right). Ab., antibodies

3.2.7. S100A4 INCREASES RANKL EXPRESSION IN RA SYNOVIAL FIBROBLASTS

A series of studies has demonstrated that RANKL is predominantly induced by synovial fibroblasts in RA (53-55). Thus, I investigated influence of S100A4 on RANKL expression in synovial fibroblasts collected from RA patients who underwent joint-replacement surgery. Five days after S100A4 treatment, synovial fibroblasts of patient #1 expressed more RANKL than those with the vehicle treatment (Figure 35A). However, synovial fibroblasts of patient #2 did not respond to S100A4 stimulation at any days of the test (Figure 35A right). I also tested a short time response to S100A4. Synovial fibroblasts of patient #3 started to express more RANKL at 24-hour after S100A4 stimulation (Figure 35B).

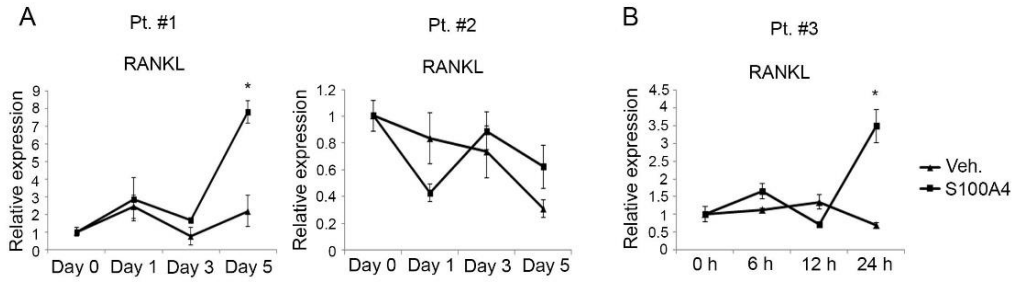

Figure 35. S100A4 increased RANKL expression from synovial fibroblasts of RA patients.

(A) Synovial fibroblasts collected from RA patient #1 (Pt. #1) and RA patient #2 (Pt. #2) were cultured for indicated days with vehicle or S100A4 (1 μg/ml) treatment and subjected to real-time PCR analyses for RANKL expression. (B) Synovial fibroblasts collected from RA patient #3 (Pt. #3) were cultured for indicated time with vehicle or S100A4 (1 μg/ml) treatment and subjected to real-time PCR analyses for RANKL expression. Pt., patient

3.3. EFFECT OF CANCER-INDUCED S100A4 ON OSTEOCLASTS

3.3.1. CHARACTERIZATION OF BONE METASTASIZED CANCERS

I established bone-metastasized breast and prostate cancer cell lines by intracardiacly injecting MDA-MB-231 (MDA) and PC3 into athymic mice. After 8 to 12 weeks of the initial injection, whole tibiae and femurs were flushed and cancer cells were selected by culturing cells for 2 months, thereby only the immortalized cancer cells survived and remained in the culture. I again injected these selected cells intracardiacly and re-established bone-metastasized cancer cells (Figure 36). Finally, I named these in vivo selected cells as bone metastasized MDA (mtMDA) and PC3 (mtPC3). To prove these cells actually were human cells by FACS analysis, the cells were labeled with human leukocyte antigens (hHLA) (Figure 36 right). Interestingly, x-ray image analyses demonstrated that bone loss in mice by mtMDA injection was more severe than that of MDA or PBS injection (Figure 36 left lower).

The bone-metastasized cancer cells were characterized in several aspects. BrdU labelling assay was performed to assess the proliferation of established cell lines. PC3 and mtPC3 proliferated in a similar rate for indicated days of culture and the same tendency was observed with MDA and mtMDA (Figure 37). Since epithelial to mesenchymal transition (EMT) is a frequently observed phenomenon in tumor metastasis (27, 28), I evaluated EMT status of the established cell lines

(Figure 38). Non-metastatic LNCaP and MCF7 cancer cell lines expressed more epithelial markers (E-cadherin, β-catenin) than mesenchymal markers (N-cadherin, snail2, vimentin), while PC3 and MDA expressed more mesenchymal markers. Interestingly, mtPC3 and mtMDA did show mesenchymal characters at even higher levels than PC3 and MDA, shown by elevated levels of vimentin and down-regulated levels of E-cadherin and β-catenin (Figure 38). A number of studies demonstrated that the NF-κB activation is an important determinant of metastasis in prostate cancer (29, 35). Thus, we assessed phosphorylations of p65, IKKαβ and IκB by Western blotting and observed more phosphorylations of p65, IKKαβ and IκB in mtPC3 than PC3 and LNCaP (Figure 39). Notably, we did not observe the NF-κB activation in mtMDA (Figure 39).

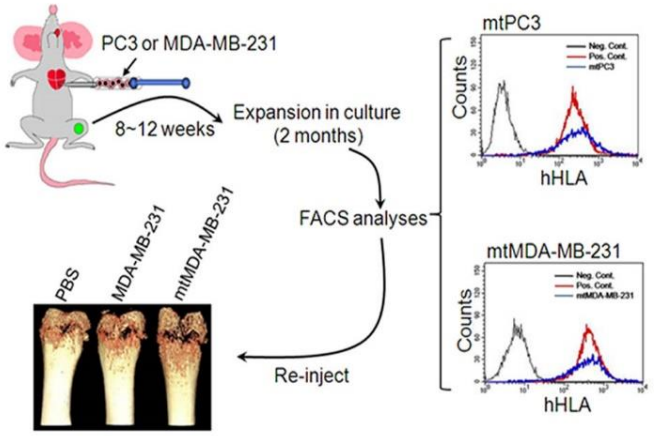

Figure 36. In vivo selection of bone metastasized cancer was performed.

A schematic diagram describing in vivo selection of bone metastasized PC3 and MDA-MB-231 (left). Briefly, intracardiacly injected cancer cells were flushed out from bones after 8 to 12 weeks and expanded in in vitro culture dishes for 2 months. Then, the cells were trypsinized and re-injected for 2nd round of selection. A representative image of bone metastasized femurs was shown by x-ray analysis (left lower). Using flow cytometry after labelling hHLA, isolation of human cancer cells was confirmed (right). Mouse bone marrow cells and human embryonic kidney cells were used as negative and positive controls, respectively. mtPC3, bone metastasized PC3 after 2nd round of in vivo selection. mtMDA-MB-

231, bone metastasized MDA-MB-231 after 2nd round of in vivo selection. hHLA, human leukocyte antigens.

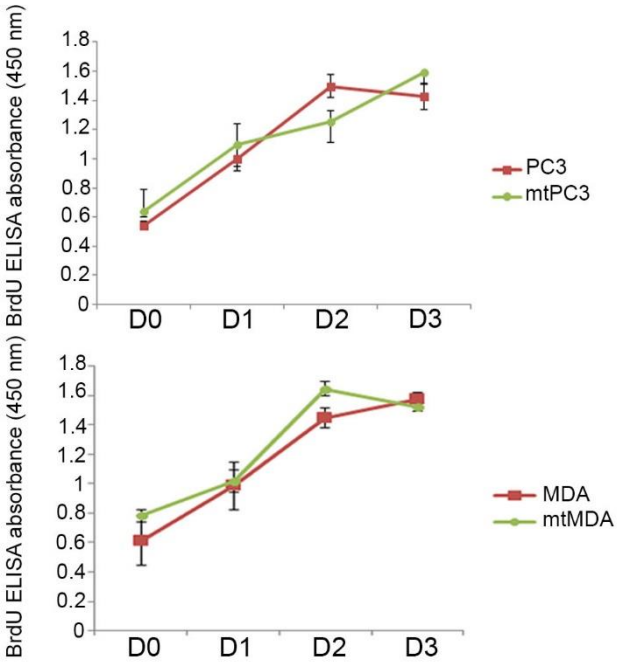

Figure 37. Proliferation of parental cells and bone metastasized cancer cells were comparable.

Proliferation of parental and bone metastasized cell lines was compared by BrdU assay. mtMDA, mtMDA-MB-231.

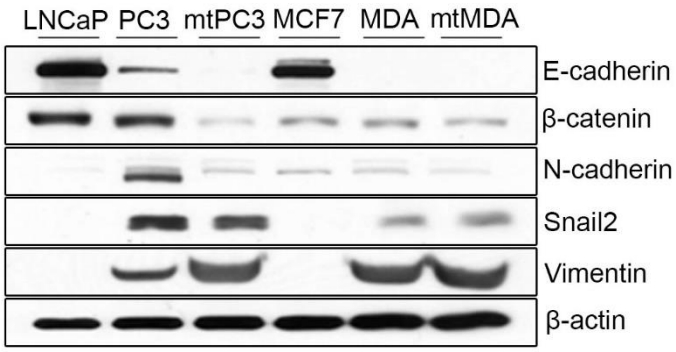

Figure 38. Epithelial to mesenchymal transition was observed in bone metastasized cancer cells.

The protein levels of epithelial (E-cadherin and β-catenin) and mesenchymal (N-cadherin, Snail2, and Vimentin) markers were assessed by Western blotting. β-Actin was included as a loading control.

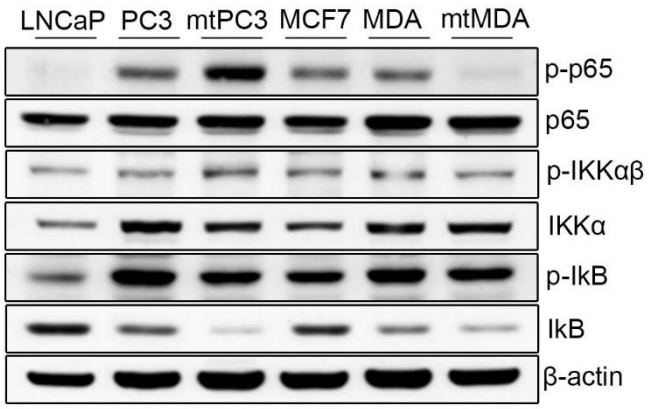

Figure 39. The NF-κB activation was observed in bone metastasized prostate cancer cells but not in breast cancer cells.

The protein levels of p-p65, p65, p-IKKαβ, IKKα, p-IκB, and IκB were assessed from indicated cancer cells by Western blotting. β-Actin was included as a loading control.

3.3.2. BONE METASTASIZED CANCER CONDITIONED MEDIUM INDUCES OSTEOCLASTOGENESIS

Accumulating evidence suggested that bone metastases accompany severe bone loss due to over-activated osteoclasts (2). Therefore, I tested whether the established cell lines stimulate osteoclastogenesis from mouse BMMs. I collected conditioned media (CM) from PC3, mtPC3, MDA and mtMDA to investigate influences of tumor secreted cytokines or proteins on osteoclastogenesis. I observed significant increases in numbers of multinucleated osteoclasts and osteoclast surface areas in mtPC3 and mtMDA CM treated groups in comparison with the PC3 and MDA CM treated groups (Figure 40). I observed that RANKL expression in mtPC3 and mtMDA was higher than the expression of PC3 and MDA (data not shown). Thus, I treated human osteoprotegerin (OPG), a decoy receptor of RANKL, to block secreted RANKL from the established cell lines. Surprisingly, OPG treatment could not completely block the increases by mtPC3 or mtMDA CM to the levels of PC3 or MDA CM, indicating the existence of factors other than RANKL affecting osteoclastogenesis in mtPC3 and mtMDA CM (Figure 41).

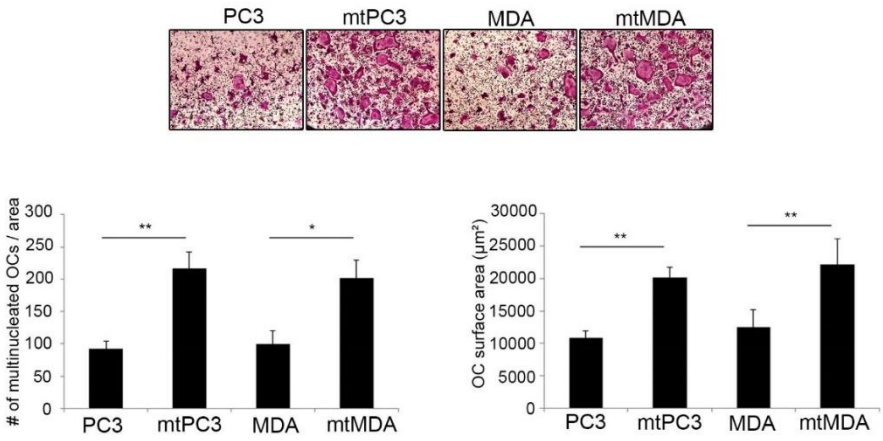

Figure 40. Bone metastasized cancer conditioned medium enhanced osteoclastogenesis.

pOCs were differentiated into mature osteoclasts by adding indicated cancer CM to the culture media (3:7, CM to fresh culture media) with M-CSF (30 ng/ml). TRAP staining was performed and TRAP-positive cells with 3 or more nuclei were counted (lower left). The surface area of mature osteoclasts was measured (lower right).

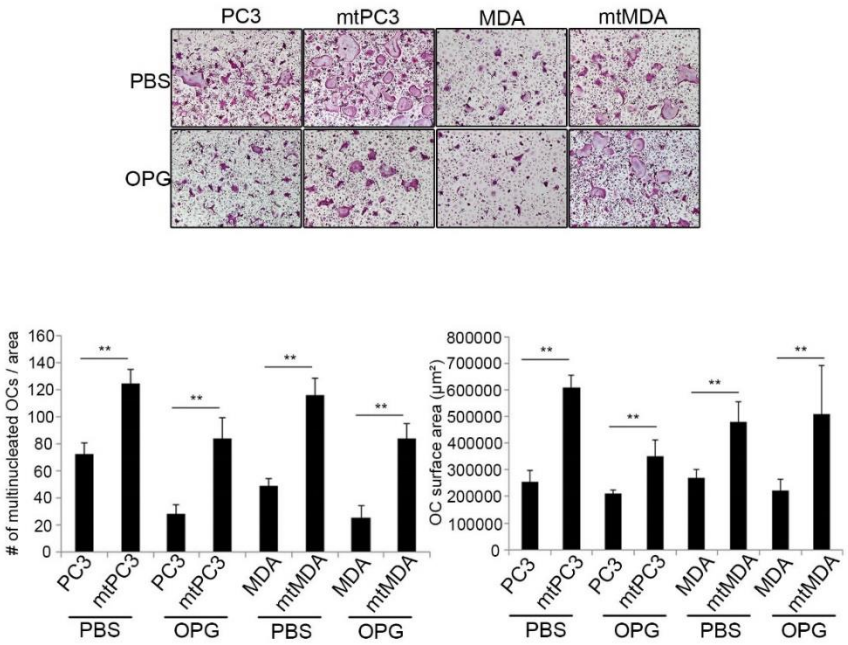

Figure 41. OPG treatment could not completely block accelerated osteoclast differentiation that was induced by bone metastasized cancer CM.

pOCs were differentiated into mature osteoclasts by adding indicated cancer CM to the culture media with M-CSF (30 ng/ml) in the presence of OPG or PBS. TRAP staining was performed and TRAP-positive cells with 3 or more nuclei were counted (lower left). The surface area of mature osteoclasts was measured (lower right).

3.3.3. ELEVATED EXPRESSION OF S100A4 IN BONE METASTASIZED CANCERS

I performed a cDNA microarray to analyze the gene expression patterns of MCF7 and MDA. Unlike MCF7, MDA preferentially metastasizes to the other organs, especially to the bone. S100A4 in MDA was 134.68 fold higher than that of MCF7 (Figure 42). I also analyzed data sets of cDNA microarray from GEO of NCBI data base, regarding breast tumor samples of known metastatic sites (GSE 14020). Within tumor samples of 65 patients, S100A4 were preferentially expressed in bone metastasized tumors in comparison with the tumors metastasized to other organs (Figure 43). Therefore, I questioned whether bone metastasized PC3 or MDA (mtPC3 or mtMDA) express S100A4 and compared its levels to non-metastatic cell lines such as LNCaP and MCF7. Its mRNA, protein, and secreted forms were confirmed by real-time PCR, Western blotting and human S100A4 ELISA, respectively (Figure 44-46). Interestingly, mtPC3 and mtMDA expressed the highest amounts of S100A4 among the cell lines tested (Figure 44-46). Collectively, these findings suggest that bone metastasized tumors express high levels of S100A4 both in humans and mice.

MCF7 vs. MDA-MB-231 microarray

TargetID	MCF7_Signal	MDA_Signal	MDA/MCF7
S100A4	242.529	32663	134.68
S100A6	20756.4	55709.2	2.684

Figure 42. Higher expression of S100A4 was observed in MDA-MB-231 by cDNA microarray analysis.

cDNA microarray was performed on Human HT-12 Expression BeadChip and the signals of S100A4 and S100A6 were compared between MCF7 and MDA-MB-231. Expression folds were calculated by dividing MDA-MB-231 signals by MCF7 signals.

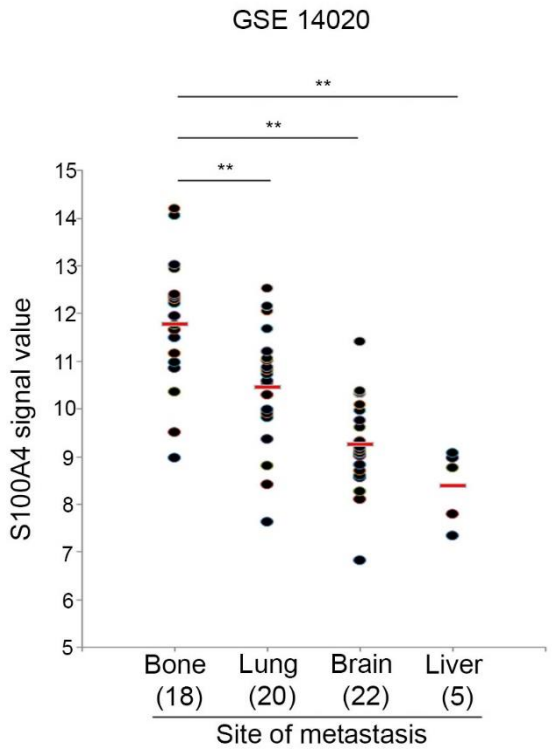

Figure 43. S100A4 were preferentially expressed in bone metastasized breast cancer.

Human S100A4 signals were analyzed from 65 breast cancer patients with known sites of metastases. The data set was retrieved from GSE 14020 of GEO data base.

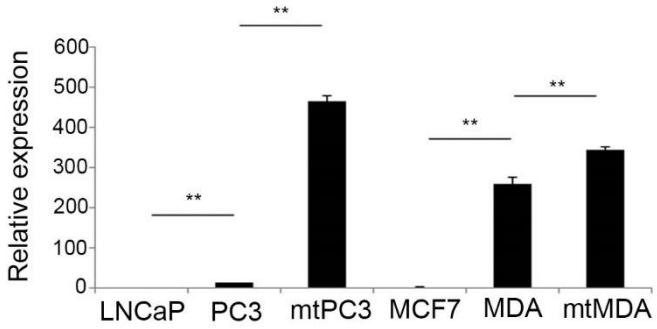

Figure 44. Elevated mRNA expressions of S100A4 in bone metastasized cancers were observed.

The expressions of S100A4 in each cancer cell lines were measured by real-time PCR. The expression of HPRT was used as an endogenous control.

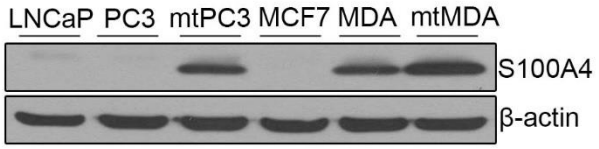

Figure 45. Elevated protein expressions of S100A4 in bone metastasized cancers were observed.

The protein levels of S100A4 in indicated cancer cell lines were assessed by Western blotting. β-Actin was included as a loading control.

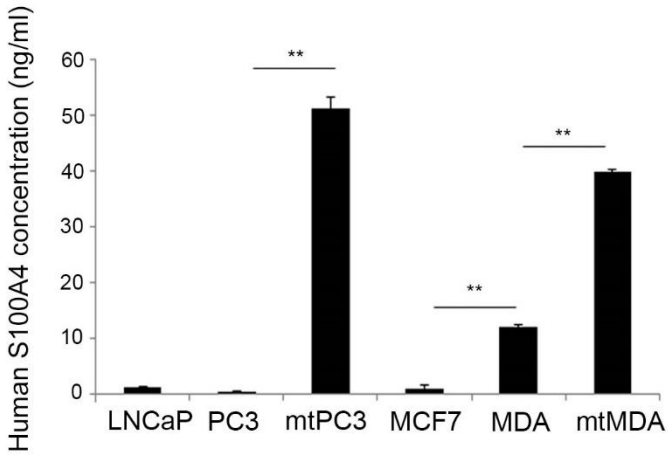

Figure 46. Secretions of S100A4 in bone metastasized cancers were increased.

In vitro culture supernatant from indicated cancer cell lines were collected. Concentrations of secreted S100A4 from each cell lines were measured by human S100A4 ELISA.

3.3.4. SECRETION OF S100A4 IS ABOLISHED BY DOWN-REGULATION OF S100A4 IN BONE METASTASIZED CANCERS

In order to find the role of increased S100A4 in bone metastasized cancer cells, I first stably down-regulated its expression by shRNA using lentiviral particles. I confirmed by Western blotting analyses that down-regulation in whole cell lysates was successfully achieved (Figure 47) and its secretion to culture media was nearly abolished (Figure 48 upper). I again confirmed this with human S100A4 ELISA (Figure 48 lower). Unlike the studies reporting the supportive roles of S100A4 in tumor progression, down-regulation of S100A4 in mtPC3 and mtMDA did not affect proliferation, migration, and invasion of cancer cells in my experiments (Figure 49 and 50).

Figure 47. ShRNA-mediated knock-down of S100A4 was achieved in bone mentastasized cancers.

ShRNA-mediated knock-down of S100A4 in mtPC3 and mtMDA was assessed by Western blotting. β-Actin was included as a loading control.

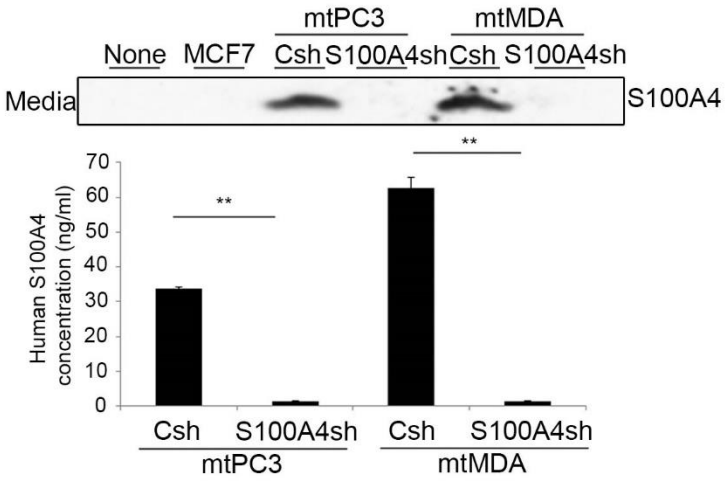

Figure 48. Secretion of S100A4 was abolished by down-regulation of S100A4 in bone metastasized cancers.

The levels of secreted S100A4 from culture media of each cell lines were determined by Western blotting (upper) and human S100A4 ELISA (lower).

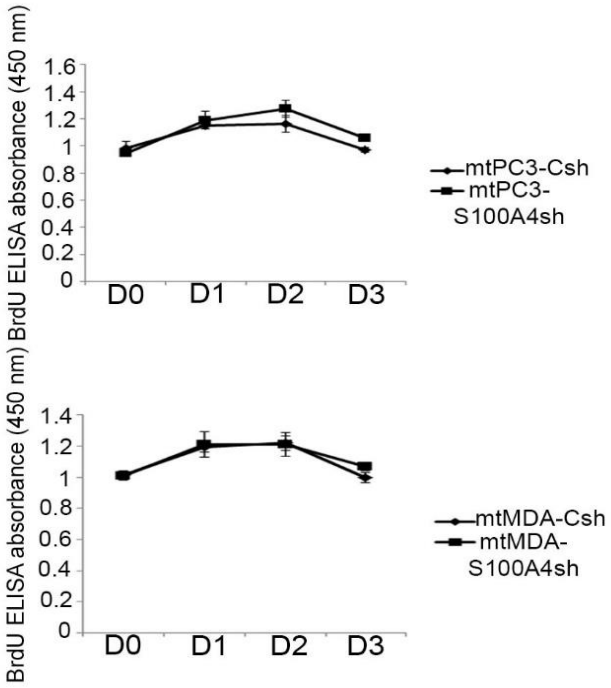

Figure 49. S100A4 knock-down did not influence the proliferation of bone metastasized cancer cells.

Proliferation of mtPC3-Csh/S100A4sh (upper) and mtMDA-Csh/S100A4sh (lower) was assessed for indicated days by BrdU assay. The absorbance was measured at 450 nm.

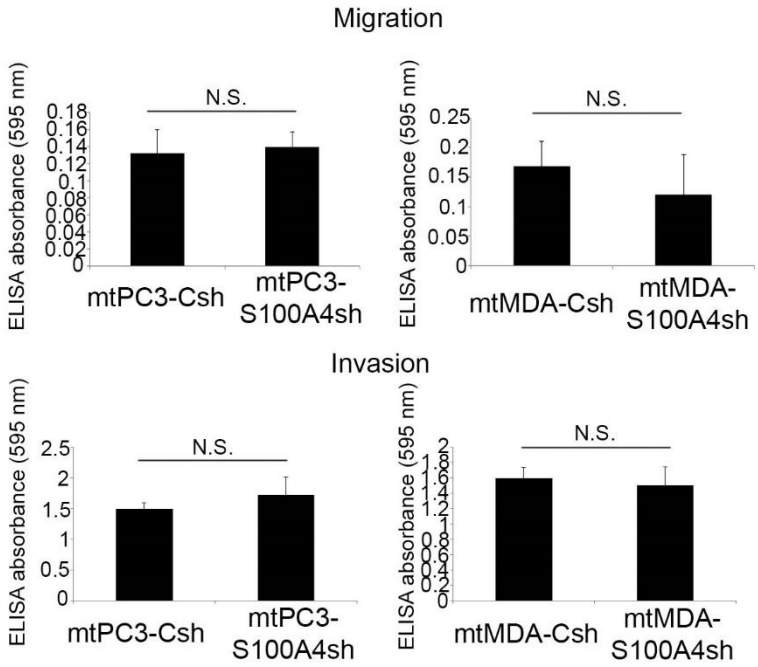

Figure 50. S100A4 knock-down did not influence the migration and invasion of bone metastasized cancer cells.

Cell migration and invasion were tested using trans-well migration assay kit and cell invasion assay kit, respectively. N.S., not significant

3.3.5. DOWN-REGULATION OF S100A4 IN BONE METASTASIZED CANCERS DECREASES CANCER-INDUCED OSTEOCLASTOGENESIS

Since the down-regulation of S100A4 did not influence characteristics of tumor themselves, I supposed that the secreted S100A4 might have affected cells resident in the bone metastatic niche. In addition, overwhelming osteoclastic bone erosions were repeatedly reported in studies regarding bone metastatic animal models and patients. Therefore, I questioned whether the tumor derived S100A4 affects osteoclastogenesis. I collected CM from in vitro cultures of mtPC3-Csh, -S100A4sh, mtMDA-Csh, -S100A4sh, and MCF7. After that, pOCs were incubated with indicated percentages of CM with M-CSF and without RANKL. As shown by TRAP staining in Figure 51, Csh CM treated pOCs dose-dependently increased numbers of multinucleated osteoclasts and surface areas in comparison with none or MCF7 CM treated cultures, while S100A4sh CM treated cultures significantly decreased in the numbers and sizes (Figure 51). I again confirmed this tendency with the addition of RANKL, indicating tumor derived S100A4 enhances osteoclastogenesis independent of RANKL (data not shown). Next, bone resorbing activities of CM treated pOCs were tested on dentin slices with presence of RANKL. In line with the TRAP staining experiments, Csh-CM treated osteoclasts resorbed the bone deeper and wider, compared to cultures treated with RANKL only or S100A4sh-CM (Figure 52). To further clarify that

the down-regulation of S100A4 decreased the formation of multinucleated osteoclasts, BMMs were co-cultured with cancer cells, so they can physically interact each other. (Figure 53). This was also observed by co-culturing BMMs with osteoblasts under influence of mtPC3 CM (Figure 54).

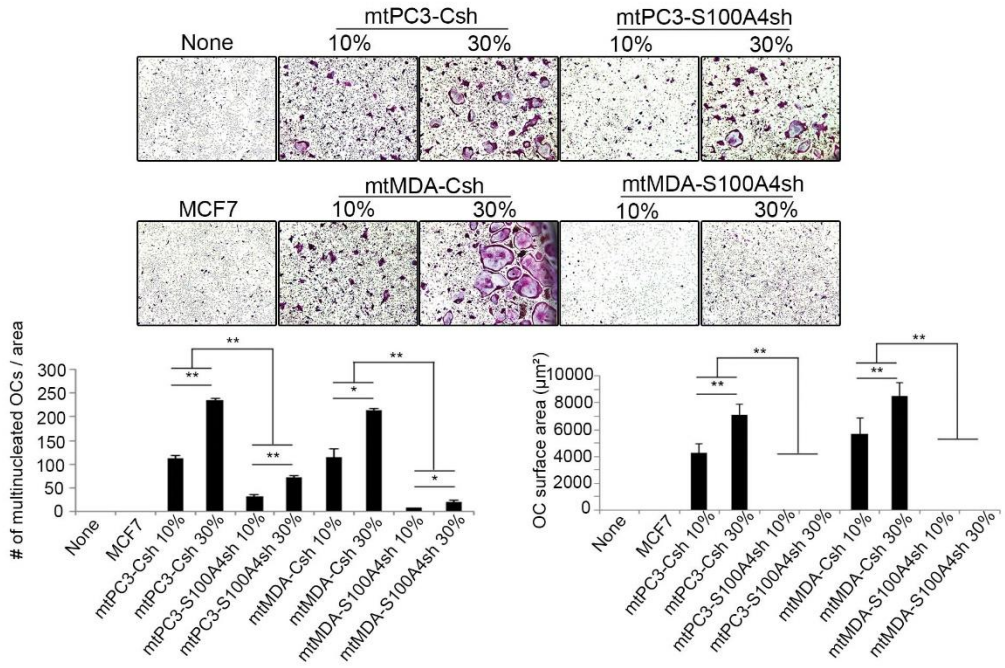

Figure 51. Down-regulation of S100A4 in bone metastasized cancer decreased cancer-induced osteoclastogenesis.

pOCs with M-CSF (30 ng/ml) were cultured with none or 10 or 30% of CM from indicated cancer cell lines and subjected for TRAP staining. Multinucleated osteoclasts and osteoclast surface areas were calculated and depicted in graphs. TRAP-positive cells with 3 or more nuclei were considered as multinucleated osteoclasts.

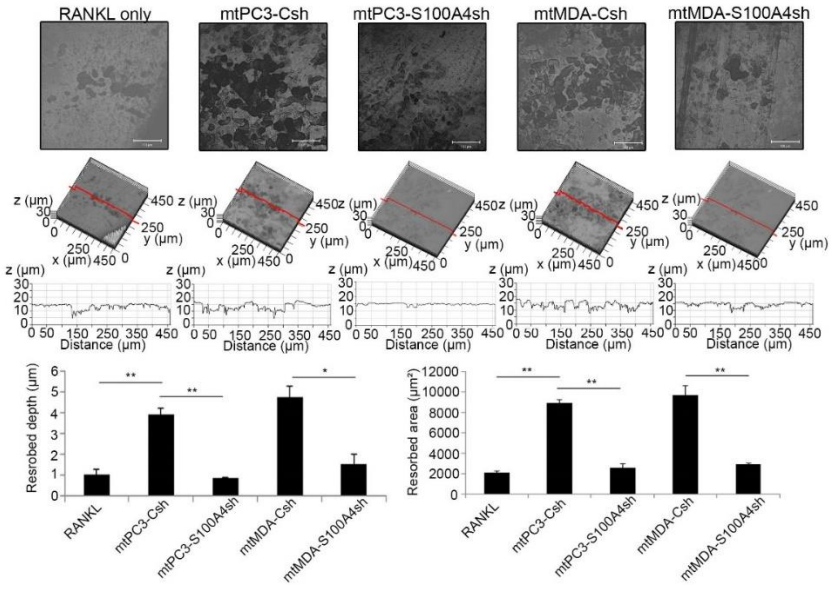

Figure 52. Down-regulation of S100A4 in bone metastasized cancers decreased bone resorption activity.

Resorbed depth and area of dentin slices were determined by culturing pOCs with 30% CM plus M-CSF (30 ng/ml) and RANKL (100 ng/ml). Dentine slices were analyzed by confocal laser microscopy. Representative images of each sample from a region on a dentine slice were shown (upper and middle). Resorbed area and depth were calculated and depicted as graphs (lower).

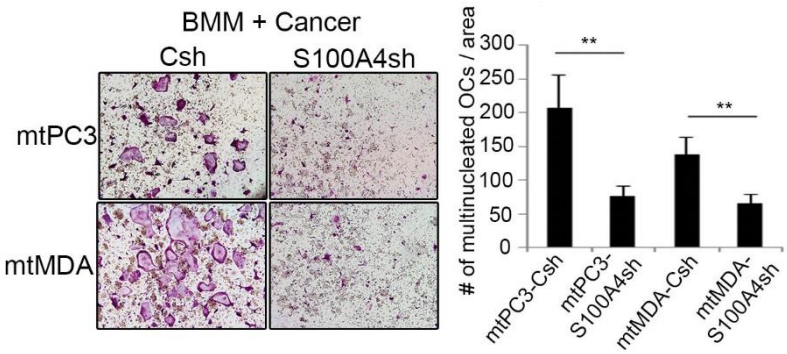

Figure 53. Down-regulation of S100A4 in bone metastasized cancers decreased cancer-induced osteoclastogenesis in cancer co-culture.

Indicated cancer cells were co-cultured with BMMs in the presence of M-CSF (30 ng/ml) and RANKL (100 ng/ml) to induce osteoclast differentiation and subjected for TRAP staining. Representative images were shown (left). TRAP-positive cells with 3 or more nuclei were counted (right).

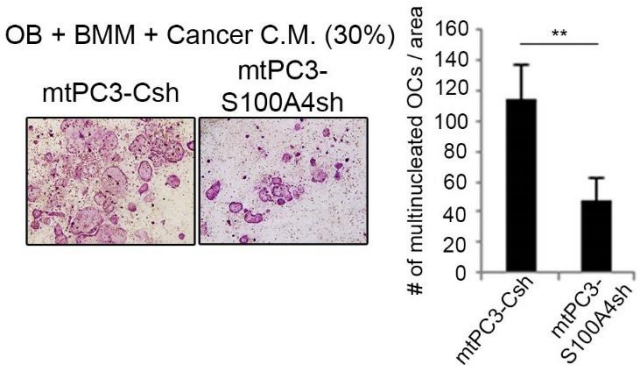

Figure 54. Down-regulation of S100A4 in bone metastasized cancer CM decreased cancer-induced osteoclastogenesis in osteoblast co-culture. BMMs co-cultured with calvarial osteoblasts (OB) in 30% of cancer CM were induced to differentiate into osteoclasts and subjected for TRAP staining. Representative images were shown (left). TRAP-positive cells with 3 or more nuclei were counted (right).

3.3.6. S100A4 POSITIVELY REGULATES OSTEOCLASTOGENESIS THROUGH MAPK AND NF-κB ACTIVATION

Based on the observation of the increases of osteoclastogenesis by S100A4 over-expressed cancer CM, I investigated whether S100A4 protein directly influences the generation of osteoclasts. pOCs were driven to differentiate into mature osteoclasts by RANKL in the presence of variable concentrations of recombinant mouse S100A4. As shown in Figure 55, S100A4 increased the formation of osteoclasts and the osteoclast surface areas at concentrations of 1 μg/ml to 5 μg/ml (Figure 55 upper). Also, mRNA expressions of osteoclast differentiation markers such as TRAP, Atp6v0d2 and MMP2 were dramatically increased by S100A4 (Figure 55 lower). To further clarify the observation with Csh- and S100A4sh- CM, I added S100A4 neutralizing antibodies to block secreted S100A4 in CM of mtPC3 and mtMDA during osteoclasts differentiation. A great reduction in the number of multinucleated osteoclasts and the areas was observed in an antibody dose-dependent manner (Figure 56). Western blotting showed that total protein levels of NFATc1 and c-Fos, crucial transcription factors in osteoclasts, decreased obviously by S100A4sh-CM of mtPC3 and mtMDA (Figure 57A and B). Since RANKL-induced osteoclastogenesis entails activation of MAPK and NF-κB pathway, I tested whether Csh- and S100A4sh-CM from mtPC3 and mtMDA influence such activation (11). Surprisingly, serum starved

pOCs stimulated with each CM increased phosphorylations of IκB, p65, JNK, ERK, and p38 within 30 minutes (Figure 58 and 59). Notably, I observed delayed and decreased phosphorylations of IκB, p65, JNK, and ERK by S100A4sh-CM of mtPC3 (Figure 58). With mtMDA-S100A4sh-CM, I observed decreases in IκB, p65, and p38 phosphorylations (Figure 59).

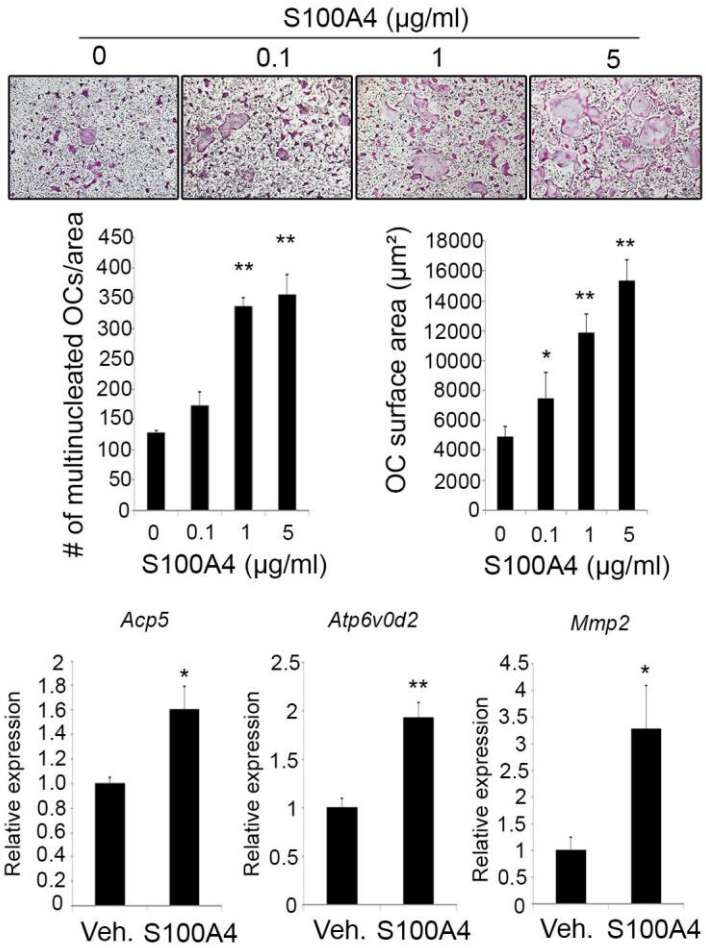

Figure 55. Recombinant S100A4 increased osteoclast differentiation.

pOCs treated with various concentrations of recombinant mouse S100A4 proteins were TRAP stained (upper). TRAP-positive cells with three or more numbers of nuclei were counted and OC surface area were measured (middle). Expression levels of osteoclast marker genes were assessed by real-time PCR analyses after S100A4 (1 μg/ml) or vehicle treatment (lower).

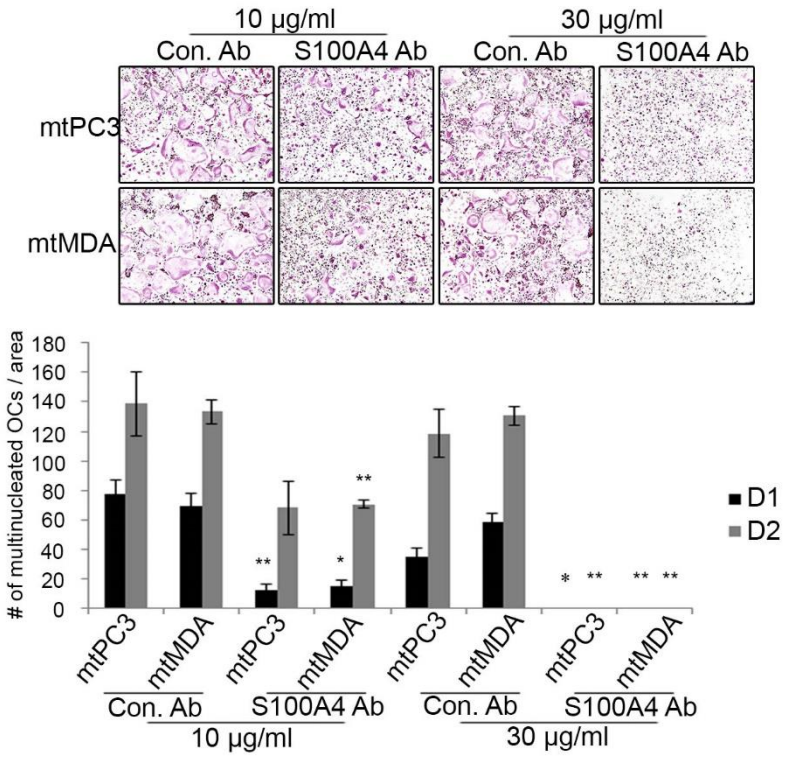

Figure 56. Neutralization of S100A4 abrogated cancer-induced osteoclastogenesis.

mtPC3 or mtMDA CM (30%) treated pOCs were cultured with 10 or 30 µg/ml of control or S100A4 neutralizing antibodies. TRAP staining was performed on day 1 and 2 after CM and antibodies treatments. Representative images of day 2 cultures were shown (upper). TRAP positive cells with three or more numbers of nuclei were counted (lower).

A

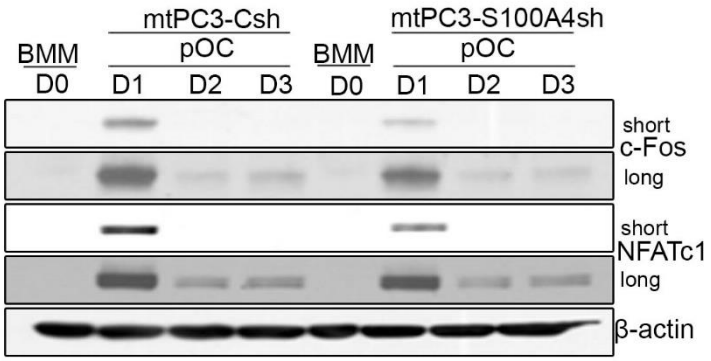

B

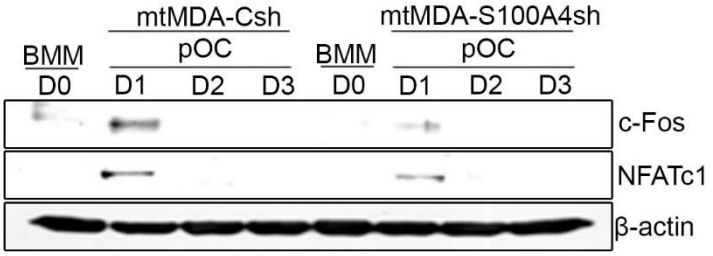

Figure 57A and B. S100A4sh-CM decreased the induction of c-Fos and NFATc1.

Whole cell lysates of pOCs treated with mtPC3-Csh/-S100A4sh (A) or mtMDA-Csh/-S100A4sh (B) CM were immunoblotted with c-Fos and NFATc1 antibodies. 30% of cancer CM was used. β-Actin was included as a loading control.

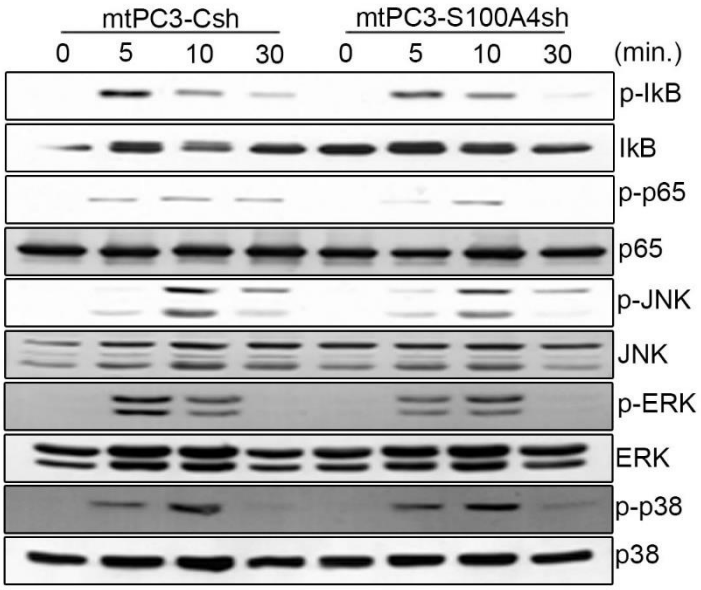

Figure 58. Phosphorylations of IκB, p65, JNK, and ERK by mtPC3-S100A4sh-CM were decreased.

pOCs were serum-starved for 4 hours followed by mtPC3-Csh or -S100A4sh CM stimulation for the indicated time. Cancer CM was mixed with fresh media in 1 to 1 ratio. The protein levels of p-p65, p65, p-IκB, IκB, p-JNK, JNK, p-ERK, ERK, p-p38, and p38 were assessed by Western blotting.

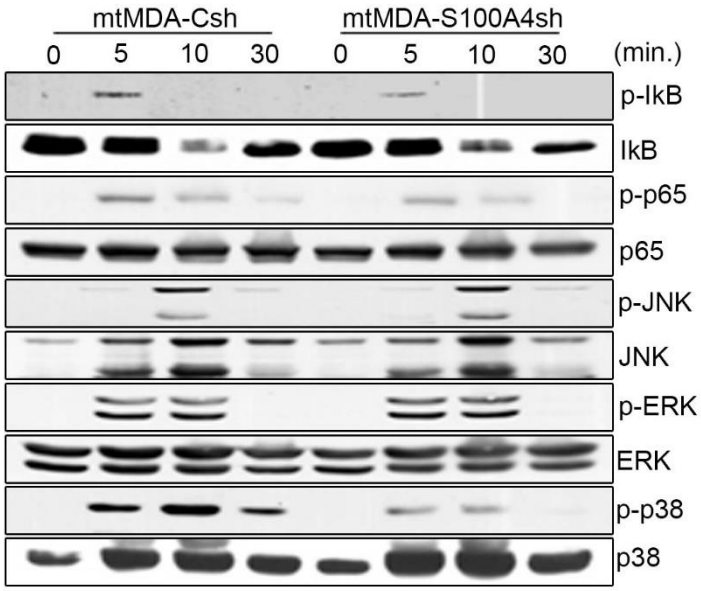

Figure 59. Phosphorylations of IκB, p65, and p38 by mtMDA-S100A4sh-CM were decreased.

pOCs were serum-starved for 4 hours followed by mtMDA-Csh or -S100A4sh CM stimulation for the indicated time. Cancer CM was mixed with fresh media in 1 to 1 ratio. The protein levels of p-p65, p65, p-IκB, IκB, p-JNK, JNK, p-ERK, ERK, p-p38, and p38 were assessed by Western blotting.

3.3.7. S100A4 ENHANCES OSTEOCLASTOGENESIS THROUGH RAGE, NOT THROUGH TLR4

As candidate receptors S100A4 regulates with which osteoclast differentiation, RAGE and TLR4 were considered. Both receptors were reported to modulate S100 protein family signaling in other type of cells (17, 24). The number of multinucleated osteoclasts formation was compared after treating TLR4 knock-out and RAGE down-regulated pOC with recombinant mouse S100A4. There was a significant decrease with RAGE down-regulation (Figure 61), while there was no significant change with TLR4 knock-out (Figure 60), indicating S100A4 enhanced osteoclastogenesis through RAGE (Figure 60 and 61). RAGE down-regulated pOCs treated with Csh- or S100A4sh-CM of mtPC3 and mtMDA were tested (Figure 62 and 63). We observed decreases in numbers of multinucleated osteoclasts and surface areas by S100A4sh-CM treatment or RAGE down-regulation in pOCs, demonstrating pivotal roles of S100A4 and RAGE in cancer-induced osteoclastogenesis (Figure 62 and 63). In addition, RAGE down-regulated pOCs treated with mtPC3 CM decreased resorbed depth and areas (Figure 64). Finally, reductions in total protein levels of c-Fos and NFATc1 were seen when mtPC3 or mtMDA CM was treated in RAGE down-regulated pOCs (Figure 65).

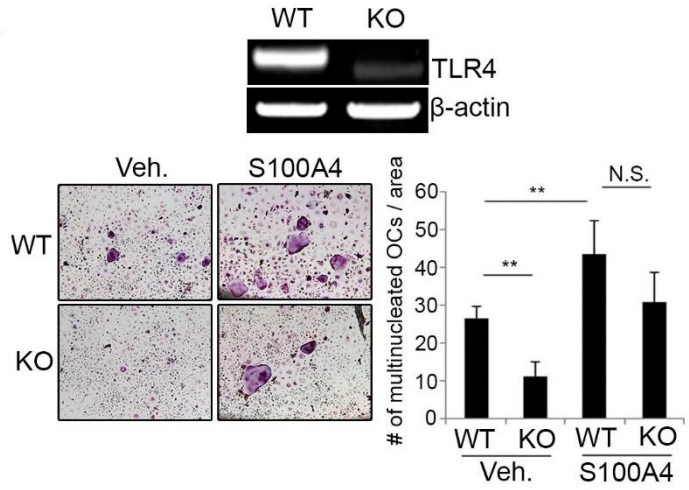

Figure 60. S100A4 did not enhance osteoclastogenesis through TLR4. TLR4 mRNA expressions in WT and TLR4 knock-out (KO) BMMs were analyzed by RT-PCR. Expression levels of β-actin were assessed for endogenous control (upper). Vehicle (Veh.) or S100A4 (1 μg/ml) treated WT or TLR4 KO pOCs were differentiated into mature osteoclasts and subjected to TRAP staining (lower left). TRAP positive cells with three or more numbers of nuclei were counted (lower right).

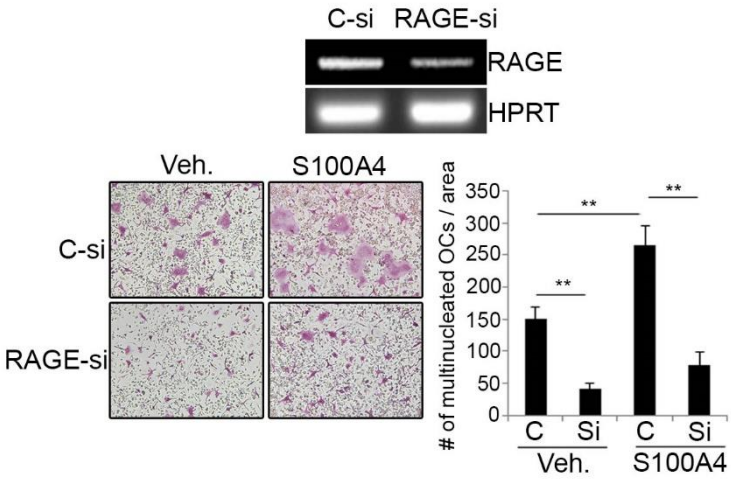

Figure 61. S100A4 enhanced osteoclastogenesis through RAGE.

BMMs transfected with C-si or RAGE-si were analyzed by RT-PCR for RAGE and HPRT expression (upper). Csi or RAGE-si transfected pOCs treated with vehicle (Veh.) or S100A4 (1 μg/ml) were differentiated into mature osteoclasts and subjected to TRAP staining (lower left). TRAP positive cells with three or more numbers of nuclei were counted (lower right).

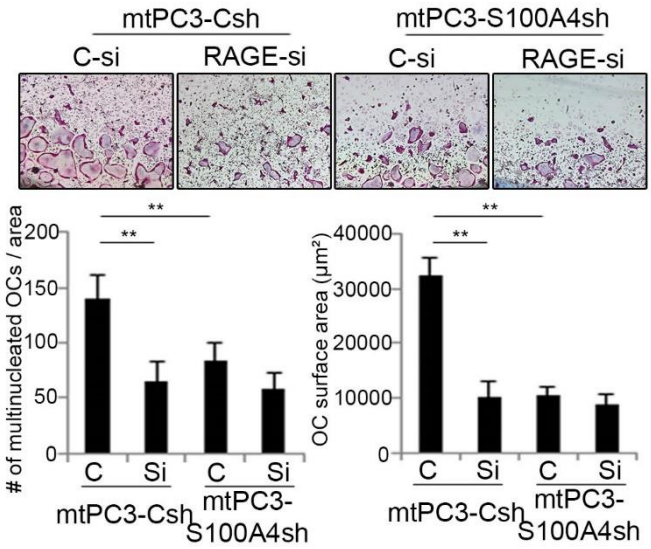

Figure 62. mtPC3-S100A4sh-CM treatment or RAGE down-regulation in pOCs decreased numbers of multinucleated osteoclasts and surface areas.

BMMs transfected with C-si or RAGE-si were differentiated into pOCs and further differentiated into mature osteoclasts by adding mtPC3-Csh or –S100A4sh CM. Representative images of TRAP-stained cells were shown (upper). TRAP-positive cells with three or more numbers of nuclei were counted and OC surface area were measured (lower).

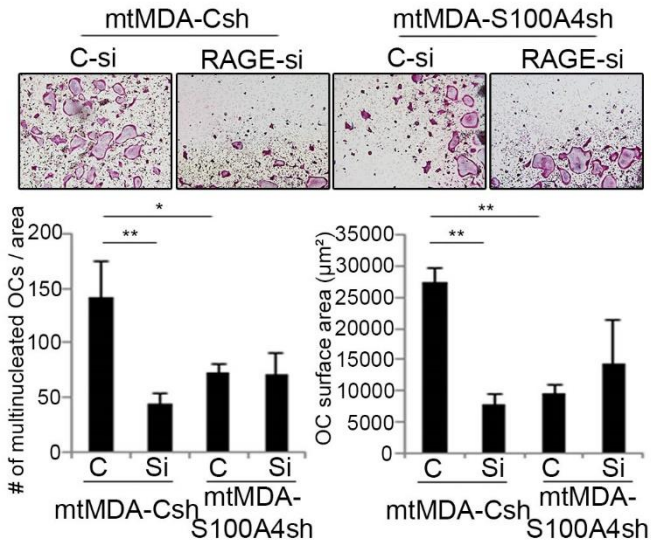

Figure 63. mtMDA-S100A4sh-CM treatment or RAGE down-regulation in pOCs decreased numbers of multinucleated osteoclasts and surface areas.

BMMs transfected with C-si or RAGE-si were differentiated into pOCs and further differentiated into mature osteoclasts by adding mtMDA-Csh or –S100A4sh CM. Representative images of TRAP-stained cells were shown (upper). TRAP-positive cells with three or more numbers of nuclei were counted and OC surface area were measured (lower).

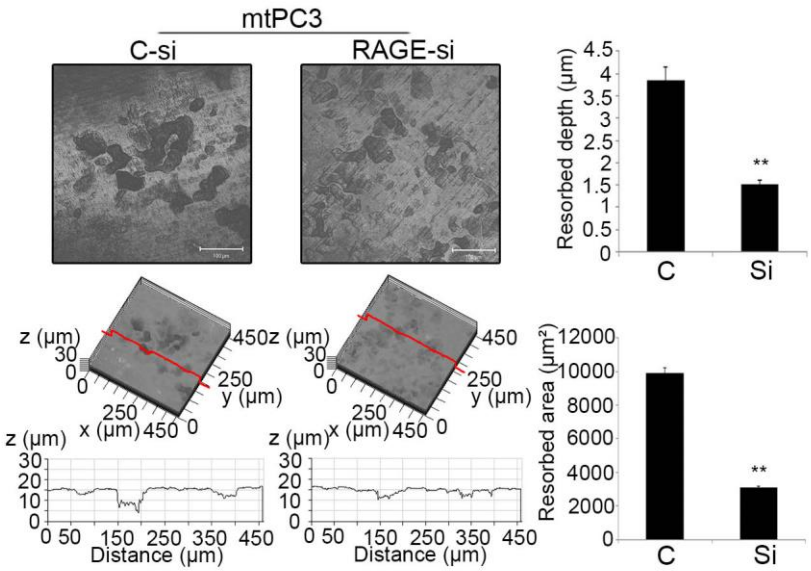

Figure 64. RAGE down-regulated pOCs treated with mtPC3 CM decreased resorbed depth and areas of dentine.

BMMs transfected with C-si or RAGE-si seeded on dentin slices were differentiated into pOCs and further differentiated into mature osteoclasts by adding mtPC3-Csh or –S100A4sh CM in the presence of M-CSF and RANKL. Dentine slices were analyzed by confocal laser microscopy. Representative images of each sample from a region on a dentine slice were shown (left). Resorbed area and depth were calculated and depicted as graphs (right).

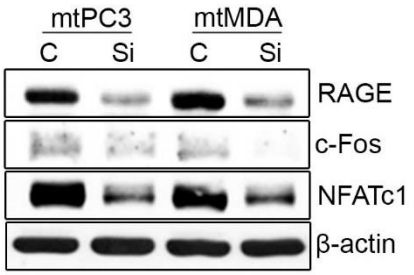

Figure 65. Reductions in total protein levels of c-Fos and NFATc1 were observed when RAGE down-regulated pOCs were treated with mtPC3 or mtMDA CM.

BMMs transfected with C-si or RAGE-si were cultured with M-CSF and RANKL to induce pOCs and cultured for an additional 1 day with mtPC3 or mtMDA CM. Cell lysates were subjected to Western blotting to detect protein levels of RAGE, c-Fos, NFATc1, and β-actin. C, C-si; Si, RAGE-si.

3.3.8. DOWN-REGULATION OF S100A4 IN BONE METASTASIZED PC3 PROTECTS BONE EROSION

To evaluate the in vivo relevance of S100A4 down-regulation in bone metastasized cancer, I intracardiacly injected 10^4 cells of mtPC3-Csh or -S100A4sh into male balb-c/nude mice. 8 weeks after the injection, mice were sacrificed and femurs from each mouse were analyzed by micro-CT scan and histochemistry. Using human specific nucleolin antibody as a marker of human cells, I verified less nucleolin positive cells in mtPC3-S100A4sh injected mice, indicating less cancers in the bone marrow (Figure 66, middle panels). Moreover, I observed less TRAP+ cells from mtPC3-S100A4sh injected mice in comparison with mtPC3-Csh injected mice (Figure 66, lower panels). Finally, trabecular bone volume analysis by micro-CT scan indicated that decrease in bone volume was less pronounced in mtPC3-S100A4sh injected mice (Figure 67). Taken together, down-regulation of S100A4 in bone metastasized prostate cancer might relieve metastatic burden in the bone marrow and would eventually reduce bone erosions by osteoclasts.

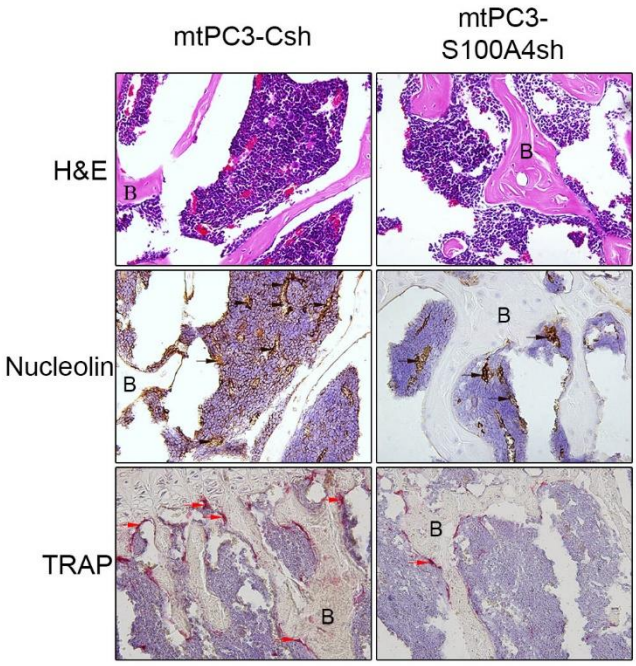

Figure 66. Intracardiac injection of S100A4 down-regulated mtPC3 decreased metastatic burden in mice femurs.

mtPC3-Csh or mtPC3-S1004sh cells were intracardiacly injected into male nude mice and sacrificed after 8 weeks for histochemistry analysis of femurs. H&E, nucleolin and TRAP staining were performed and areas underneath the growth plate were shown as representative images. Black arrows, nucleolin positive cells; Red arrows, TRAP positive cells; B, trabecular bone; H&E, hematoxylin & eosin.

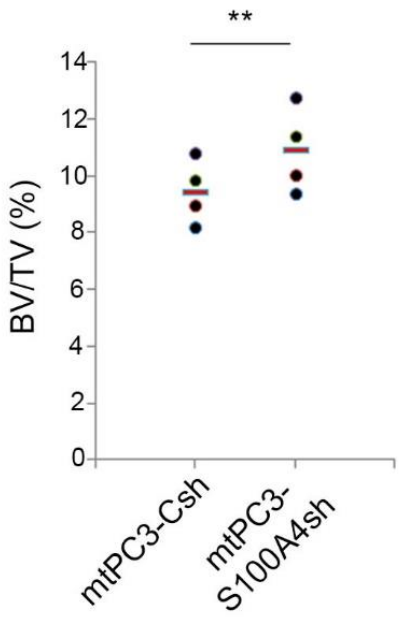

Figure 67. Intracardiac injection of mtPC3-S100A4sh protected trabecular bone of mice in comparison with mtPC3-Csh-injected mice.

After performing micro-CT analysis, trabecular bone volume over tissue volume was calculated by analyzing femurs of mtPC3-Csh or mtPC3-S100A4sh cancer-injected mice. 4 femurs from each group were analyzed (n=2 mice per group).

CHAPTER 4

DISCUSSION

4.1. EXTRACELLULAR S100A4 NEGATIVELY REGULATES OSTEOBLAST FUNCTION BY ACTIVATING THE NF-κB PATHWAY

In this part of study, I investigated the role of extracellular S100A4 in the inhibition of bone formation by activating the NF-κB pathway in osteoblasts. Although early differentiation of osteoblast was not affected (Figure 4 and 5), late-stage differentiation of osteoblast and mineralization activity were reduced by S100A4 treatment (Figure 8). Consistent with the results of my in vitro experiments, S100A4 injection onto neonatal calvariae decreased the mineral apposition rate (Figure 15). Mechanistically, the NF-κB activation in osteoblasts by S100A4 seems to be responsible for the inhibition of bone formation (Figure 11-13).

Bone-loss in inflammatory conditions largely depends on enhanced bone resorption by osteoclasts and delayed bone formation by osteoblasts. Among inflammatory cytokines, TNF-α was shown to directly inhibit mineralized nodule formation and osteocalcin secretion from osteoblasts (56). Moreover, the expression of Runx2 was decreased upon TNF-α treatment (57), and TNF-α induced expression of Smad ubiquitination regulatory factor 1/2 (Smurf 1/2), which ubiquitylates Runx2 for proteasomal degradation (58). Yamazaki et al.

demonstrated that bone morphogenetic protein 2 (BMP2)-mediated activation of Smads, crucial transcription factors of osteoblast differentiation, was abrogated by TNF-α via NF-κB activation (39). Moreover, the activation of NF-κB by TNF-α induced cAMP response element-binding protein H (CREBH), which in turn up-regulated Smurf 1 to inactivate the Smad/Runx2 regulatory system (59). Mice specifically overexpressing the dominant negative form of IKK in osteoblasts displayed increased bone mass (37). These studies are in accordance with my finding of S100A4 mediating inhibition of mineralization through the activation of NF-κB and strongly support a negative correlation between bone anabolism and the activation of NF-κB in osteoblasts.

It was previously demonstrated that the synovial fluids of RA patients had mean concentration of 1.98 μg/ml of S100A4 which was significantly higher than the concentration of 0.247 μg/ml in osteoarthritis patients (31). Since RA promotes and maintains a more inflamed condition near the articular joints than osteoarthritis, the effect of extracellular S100A4 on bone cells might be more pronounced in RA. In a previous study, I determined that S100A4 was secreted from lipopolysaccharide-stimulated human periodontal ligament cells, supporting the possibility of S100A4 regulation of bone cells in inflammatory diseases (60). The concentrations of recombinant S100A4 used in this study for the in vitro tests

were 1 or 2 μg/ml, which are similar to the level found in the inflammatory environment in arthritis patients.

Here, I described the effect of extracellular S100A4 on the activation of the NF-κB pathway. Finding receptor(s) that mediate activation in osteoblasts is an interesting subject of further study. RAGE and TLR4 are the two most well characterized receptors for S100A4 in a variety of cell types (61-64). NF-κB signaling in peripheral blood mononuclear cells was shown to be activated by S100A4 via TLR4 (61), while a series of studies demonstrated that S100A4 mediates signals via RAGE, especially in cancer cells (62-64). Both receptors are critical components of the NF-κB signaling pathway.

In conclusion, my study demonstrates that extracellular S100A4 interrupts the mineralization function of osteoblasts and causes an imbalance in bone homeostasis by inhibiting new bone formation. Here, I showed for the first time that this phenomenon is mediated through NF-κB activation.

4.2. EXTRACELLULAR S100A4 POSITIVELY REGULATES OSTEOCLASTOGENESIS AND OSTEOCLAST FUNCTION BY ACTIVATING THE NF-κB PATHWAY

In this part of the study, I report that extracellular S100A4 stimulates osteoclast differentiation and activation. As reported by previous studies and in my RA patient samples, a high concentration of S100A4 existed in RA patient. This can possibly cause imbalanced bone homeostasis by direct targeting of osteoclasts. Therefore, I speculated that S100A4, especially its extracellular form in the inflamed synovia of RA, might play an important role in RA bone erosion through osteoclast activation.

Previous researchers reported that S100A4 was up-regulated in cells residing in RA synovial tissues (31). This observation was further supported by blood samples of RA patients expressing higher levels of S100A4, observed in GDS2952 data set from NCBI GEO data base (Figure 16). It should be noted that RA patients still sustained the high S100A4 expression even after the anti-TNF (Enbrel) treatment (Figure 16). To further investigate, I collected synovial fluid of RA and OA patients and confirmed higher concentration of S100A4 existed in RA (Figure 17). Finally, I demonstrated that recombinant mouse S100A4 injection

onto mice calvaria bones caused bone destruction and increased number of TRAP-positive osteoclasts (Figure 19 and 21). This led to conclude that excessive amounts of extracellular S100A4 in synovial fluid or blood vessels that cross the synovium may promote bone erosion.

To study the direct induction of osteoclastogenesis by exogenous S100A4, I differentiated pOCs into mature osteoclasts with mouse recombinant S100A4. S100A4 addition resulted in acceleration of multinucleated osteoclasts formation and resorption. Osteoclast markers, such as cathepsin K, DC-STAMP and MMP-9, were induced by the S100A4 stimulation as well. Especially, MMPs, destroyers of tissue matrix, were known to be up-regulated by S100A4 in breast and prostate cancers and RA synovial tissues (51, 52, 65). Thus, I suggest that osteoclasts express MMP-9 upon S100A4 stimulation and this could deteriorate RA even more. In addition, S100A8, which is known to exist at an elevated level in RA, enhanced osteoclastic bone resorption by changing the shape of the osteoclasts, while it was not able to induce osteoclast markers (30). This suggests that S100A4 is even more potent than S100A8 due to its potential to induce osteoclast marker genes as well as osteoclast activation.

In chondrocytes, extracellular S100A4 binds RAGE to activate ERK and the NF-κB pathway (32). Therefore, I tested the possibility of S100A4 in activation of such pathways in osteoclasts. First, I identified S100A4 activation of

MAPK and NF-κB in osteoclasts (Figure 24) and then we confirmed the RAGE expression in RANKL-induced osteoclasts (Figure 27). Next, I observed that down-regulation of RAGE in osteoclasts reduced the NF-κB activation by S100A4 stimulation (Figure 29). Finally, this was further validated by a decrease in osteoclasts formation and markers (Figure 28 and 30). Since I observed S100A4 inhibition in the early stage of osteoclastogenesis, I assumed that S100A4-induced osteoclastogenesis requires expression of RAGE, which is absent in the early stage but present in the middle to late stage of osteoclastogenesis (Figure 27). It should be taken into consideration that RAGE down-regulation still retained the activation of ERK and Akt (data not shown), indicating S100A4 can still mediate signals through other receptors.

A series of reports demonstrated that activated macrophages, fibroblasts, leukocytes, and endothelial cells secreted S100A4 under pathological conditions such as RA (31, 51). In my study, the expression of S100A4 in osteoclast precursors increased upon RANKL stimulation and its secretion was more remarkable (Figure 31 and 32). Neutralizing secreted S100A4 abolished osteoclast differentiation (Figure 34), indicating S100A4 as a requisite element of osteoclastogenesis. Taken together, the increased number of osteoclasts in RA may contribute to enhanced S100A4 availability in synovial fluid and blood

vessels, which in turn accelerates other cells to secrete inflammatory factors such as metalloproteinases (65).

A number of studies showed synovial fibroblasts as a main source of RANKL in RA (53-55). Thus, I checked whether S100A4 influenced RANKL expression in synovial fibroblasts from RA patients. Surprisingly, enhanced RANKL expression was observed in both long and short-term culture conditions of RA synovial fibroblasts by S100A4 stimulation (Figure 35). These results suggest that the S100A4-rich circumstance in RA not only enhances osteoclastogenesis directly, but also stimulates other cells such as synovial fibroblasts to increase RANKL secretion to support osteoclastogenesis indirectly.

In conclusion, extracellular S100A4 in RA directly enhances osteoclastogenesis through RAGE, followed by the NF-κB activation. Moreover, activated osteoclasts secrete S100A4 in an autocrine manner to affect the adjacent stromal cells and synovial fibroblasts, resulting in an eventual increase in RANKL production. Taken together, I suggest that excessive amount of S100A4 in synovia greatly threatens RA patients' bone health.

4.3. CANCER-INDUCED S100A4 POSITIVELY REGULATES OSTEOCLASTOGENESIS

Most of women with advanced breast cancer and men with prostate cancer experience bone metastases and drugs that effectively cure the disease are not yet available on the market. Nowadays, bisphosphonates and denosumab are available as prescribed drugs, which work by directly targeting osteoclast other than cancers (66). However, inducing apoptosis of osteoclasts or disrupting osteoclastogenesis by these drugs leads to an imbalance of bone homeostasis due to the several roles of osteoclast (more specifically clastokines which are secreted during osteoclast differentiation and are contributed to important roles of bone homeostasis) in the bone homeostasis network (67). As mentioned earlier, the 'vicious cycle' starts when disseminated cancers from the primary site enter the bone microenvironment (20). Thus, directly targeting the cancers, which have entered the bone, might be the most effective therapy. The researchers have validated candidates such as PTHrP from bone metastasized cancers (23, 68), but the market demands more attractive targets.

In order to study tumor metastases in organs of interest, heterogeneous metastatic primary tumors at the primary site need to be separated into an organ-specific homogenous subpopulation, which chooses or favors microenvironment

of distant organs (22). To obtain such population in the bone microenvironment from an animal model, I intracardiacly injected potent metastatic prostate and breast cancer cell lines, PC3 and MDA-MB-231 respectively, into athymic mice and selected the population that metastasized in the bone microenvironment (Figure 36). These metastasized cancers, flushed out from the bone marrow, were maintained in in vitro culture and subjected for identification of bone metastatic characters (Figure 36).

Metastatic cancers experience EMT during the process of dissemination from the primary site (69). EMT is accompanied by elevated expression of mesenchymal genes, such as vimentin, and decreased expression of epithelial genes, for instance E-cadherin (70). Therefore, mimicking human metastasis in mouse model needs a further validation of what is commonly observed in human tumor metastasis. I compared the EMT state of mtPC3 and mtMDA from their parental cells, PC3 and MDA and found that mtPC3 and mtMDA have more mesenchymal characters than their parental cells (Figure 38). Recently, the NF-κB activation in bone metastatic prostate cancer is reported (71). According to the report of Jin et al., PC3 cell lines proliferated at a higher rate than LNCaP within boney metastatic lesions and this was due to an increased NF-κB activation in PC3. Furthermore, this resulted in induction of RANKL and PTHrP. Additionally, forced activation of the NF-κB in LNCaP promoted tumor formation and

osteoclastogenesis in the bone (71). In agreement with their findings, I observed more NF-κB activation in PC3 and this was more eminent in mtPC3. However, I did not observe any differences among breast cancer cell lines in terms of the NF-κB activation, indicating bone metastasis of breast cancer might be regulated through other mechanisms. Taken together, established cell lines exhibit bone metastatic characteristics in terms of EMT and the NF-κB activity.

Metastasized cancer cells are one of the producers of RANKL during bone metastasis. During prostate cancer progression, RANKL is a novel marker of EMT and this is associated with skeletal metastasis (72). For that reason, I tested osteoclastogenic potential of mtPC3 and mtMDA and observed increased formation of osteoclasts (Figure 40). Interestingly, treatment of OPG could not completely abolish the enhanced formation of osteoclasts by bone metastasized cancer CM (Figure 41), demonstrating that factors other than RANKL exist to enhance osteoclastogenesis. In an effort of finding factors besides of RANKL, I performed microarray analysis to assess a differential gene expression between non-metastatic MCF7 and highly bone metastatic MDA-MB-231. Among the genes that were significantly upregulated in MDA, S100A4 marked the highest (Figure 42). This is well correlated with my next finding from GSE 14020, which highlights a remarkable expression of S100A4 in bone metastasized breast cancer patients (Figure 43). More surprisingly, the expression of S100A4 was even more

elevated in mtPC3 and mtMDA than parental cells and non-metastatic cell lines. This phenomenon raises several questions; why do they need more S100A4 to enter the bone?; what makes them to over-express S100A4?; what is the effect of an extracellular S100A4 in the bone microenvironment? First two questions might have been answered in previous studies done by other researchers (33, 73, 74), but the last question remains to be elucidated. In order to answer the last question, I stably down-regulated S100A4 using shRNA mediated lentiviral particles in mtPC3 and mtMDA, which showed a near-complete abolishment of S100A4 secretion in culture media (Figure 48). Then, CMs from each cancer cell lines were collected and tested for osteoclastogenic potential. Interestingly, the number of osteoclast formations was greatly reduced in the absence of S100A4 secretion (Figure 51). This was further demonstrated by co-culturing osteoclasts with cancers and calvarial osteoblasts (Figure 53 and 54). Moreover, in the previous sections, I observed S100A4 as a negative regulator of osteoblast matrix mineralization and a positive regulator of RANKL expression. Consequently, S100A4 from cancers drives the bone microenvironment to be very catabolic by activating osteoclasts and impairing osteoblast function, which answers the last question.

Roles of S100A4 were reported in several studies especially in cancer. Tumor growth and dissemination can be inhibited by impeding S100A4 (33). The

expression of S100A4 was reported to be upregulated during the S-phase of the cell cycle (33). Also, S100A4 regulates cancer invasion and migration by adjusting extracellular matrix, cell membrane fluidity and cytoskeleton (33). Additionally, S100A4 enhances MMP activity by down regulating tissue inhibitor of metalloproteinases (TIMP)-2, which is an endogenous inhibitor of MMPs (33). Also, my in vitro tests demonstrated enhanced migration and invasion of mtPC3 and mtMDA in comparison with parental cell lines PC3 and MDA, respectively (manuscript in preparation). Based on these findings, I speculated that increased proliferation, migration, and invasion were due to elevated S100A4 expression in mtPC3 and mtMDA. However, down-regulating S100A4 expression in mtPC3 and mtMDA by shRNA did not show any differences in proliferation, migration, and invasion. I assumed that this disparity is because of the method, manipulating the expression of S100A4. Although I almost completely blocked the secretion of S100A4 from cancers by shRNA mediated knock-down, S100A4 might still be present intracellularly to regulate cancer behaviors.

In summary, bone metastasized prostate and breast cancers secrete a significant amount of S100A4 that could risk normal bone homeostasis. I suggested three strategies from this study, which might restore the imbalance. First of all, down-regulating the expression of S100A4 in cancer by shRNA successfully blocked the secretion of S100A4 and this effectively lowered the

increased numbers of multinucleated osteoclasts formation. Next, neutralizing secreted S100A4 by antibodies was also sufficient to block the enhancement of osteoclasts formation. Finally, down regulating RAGE, the receptor of S100A4 in osteoclast, further inhibited osteoclast differentiation and activation by S100A4. Further studies are needed to validate in vivo efficacy of three strategies I suggested.

REFERENCES

1. Becker DJ, Kilgore ML, Morrisey MA. The societal burden of osteoporosis. Curr Rheumatol Rep. 2010;12(3):186-91.

2. Manolagas SC, Jilka RL. Bone marrow, cytokines, and bone remodeling. Emerging insights into the pathophysiology of osteoporosis. N Engl J Med. 1995;332(5):305-11.

3. Kular J, Tickner J, Chim SM, Xu J. An overview of the regulation of bone remodelling at the cellular level. Clin Biochem. 2012;45(12):863-73.

4. Teitelbaum SL. Bone resorption by osteoclasts. Science. 2000;289(5484):1504-8.

5. Boyle WJ, Simonet WS, Lacey DL. Osteoclast differentiation and activation. Nature. 2003;423(6937):337-42.

6. Asagiri M, Takayanagi H. The molecular understanding of osteoclast differentiation. Bone. 2007;40(2):251-64.

7. Lee ZH, Kim H-H. Signal transduction by receptor activator of nuclear factor kappa B in osteoclasts. Biochem and Biophys Res Commun. 2003;305(2):211-4.

8. Takayanagi H, Kim S, Koga T, Nishina H, Isshiki M, Yoshida H, et al. Induction and activation of the transcription factor NFATc1 (NFAT2) integrate

RANKL signaling in terminal differentiation of osteoclasts. Dev Cell. 2002;3(6):889-901.

9. Kim JH, Kim N. Regulation of NFATc1 in Osteoclast Differentiation. J Bone Metab. 2014;21(4):233-41.

10. Bianco P, Cao X, Frenette PS, Mao JJ, Robey PG, Simmons PJ, et al. The meaning, the sense and the significance: translating the science of mesenchymal stem cells into medicine. Nat Med. 2013;19(1):35-42.

11. Karsenty G, Kronenberg HM, Settembre C. Genetic control of bone formation. Annu Rev Cell Dev Biol. 2009;25:629-48.

12. Miyazono K, Maeda S, Imamura T. BMP receptor signaling: transcriptional targets, regulation of signals, and signaling cross-talk. Cytokine Growth Factor Rev. 2005;16(3):251-63.

13. Crane JL, Cao X. Bone marrow mesenchymal stem cells and TGF-beta signaling in bone remodeling. J Clin Invest. 2014;124(2):466-72.

14. Arend WP. The innate immune system in rheumatoid arthritis. Arthritis Rheum. 2001;44(10):2224-34.

15. Zwerina J, Redlich K, Schett G, Smolen JS. Pathogenesis of rheumatoid arthritis: targeting cytokines. Ann N Y Acad Sci. 2005;1051:716-29.

16. Firestein GS. Immunologic mechanisms in the pathogenesis of rheumatoid arthritis. J Clin Rheumatol. 2005;11(3 Suppl):S39-44.

17. Brennan FM, Foey AD, Feldmann M. The importance of T cell interactions with macrophages in rheumatoid cytokine production. Curr Top Microbiol Immunol. 2006;305:177-94.

18. Choi Y, Arron JR, Townsend MJ. Promising bone-related therapeutic targets for rheumatoid arthritis. Nat Rev Rheum. 2009;5(10):543-8.

19. Weilbaecher KN, Guise TA, McCauley LK. Cancer to bone: a fatal attraction. Nat Rev Rhem. 2011;11(6):411-25.

20. Mundy GR. Metastasis to bone: causes, consequences and therapeutic opportunities. Nat Rev Cancer. 2002;2(8):584-93.

21. Roodman GD. Mechanisms of bone metastasis. N Engl J Med. 2004;350(16):1655-64.

22. Kang Y, Siegel PM, Shu W, Drobnjak M, Kakonen SM, Cordon-Cardo C, et al. A multigenic program mediating breast cancer metastasis to bone. Cancer Cell. 2003;3(6):537-49.

23. Yin JJ, Selander K, Chirgwin JM, Dallas M, Grubbs BG, Wieser R, et al. TGF-beta signaling blockade inhibits PTHrP secretion by breast cancer cells and bone metastases development. J Clin Invest. 1999;103(2):197-206.

24. Sethi N, Kang Y. Dysregulation of developmental pathways in bone metastasis. Bone. 2011;48(1):16-22.

25. Pratap J, Lian JB, Stein GS. Metastatic bone disease: role of transcription factors and future targets. Bone. 2011;48(1):30-6.

26. Heizmann CW, Fritz G, Schafer BW. S100 proteins: structure, functions and pathology. Front Biosci. 2002;7:d1356-68.

27. Roth J, Vogl T, Sorg C, Sunderkotter C. Phagocyte-specific S100 proteins: a novel group of proinflammatory molecules. Trends Immunol. 2003;24(4):155-8.

28. Emberley ED, Murphy LC, Watson PH. S100 proteins and their influence on pro-survival pathways in cancer. Biochem Cell Biol. 2004;82(4):508-15.

29. Foell D, Kane D, Bresnihan B, Vogl T, Nacken W, Sorg C, et al. Expression of the pro-inflammatory protein S100A12 (EN-RAGE) in rheumatoid and psoriatic arthritis. Rheumatology (Oxford). 2003;42(11):1383-9.

30. Grevers LC, de Vries TJ, Vogl T, Abdollahi-Roodsaz S, Sloetjes AW, Leenen PJ, et al. S100A8 enhances osteoclastic bone resorption in vitro through activation of Toll-like receptor 4: implications for bone destruction in murine antigen-induced arthritis. Arthritis Rheum. 2011;63(5):1365-75.

31. Klingelhofer J, Senolt L, Baslund B, Nielsen GH, Skibshoj I, Pavelka K, et al. Up-regulation of metastasis-promoting S100A4 (Mts-1) in rheumatoid arthritis: putative involvement in the pathogenesis of rheumatoid arthritis. Arthritis Rheum. 2007;56(3):779-89.

32. Yammani RR, Carlson CS, Bresnick AR, Loeser RF. Increase in production of matrix metalloproteinase 13 by human articular chondrocytes due to

stimulation with S100A4: Role of the receptor for advanced glycation end products. Arthritis Rheum. 2006;54(9):2901-11.

33. Sherbet GV. Metastasis promoter S100A4 is a potentially valuable molecular target for cancer therapy. Cancer Lett. 2009;280(1):15-30.

34. Boye K, Maelandsmo GM. S100A4 and metastasis: a small actor playing many roles. Am J Pathol. 2010;176(2):528-35.

35. Pathuri P, Vogeley L, Luecke H. Crystal structure of metastasis-associated protein S100A4 in the active, calcium-bound form. J Mol Biol. 2008;383(1):62-77.

36. Garrett SC, Varney KM, Weber DJ, Bresnick AR. S100A4, a mediator of metastasis. J Biol Chem. 2006;281(2):677-80.

37. Chang J, Wang Z, Tang E, Fan Z, McCauley L, Franceschi R, et al. Inhibition of osteoblastic bone formation by nuclear factor-kappaB. Nat Med. 2009;15(6):682-9.

38. Chang J, Liu F, Lee M, Wu B, Ting K, Zara JN, et al. NF-kappaB inhibits osteogenic differentiation of mesenchymal stem cells by promoting beta-catenin degradation. Proc Natl Acad Sci U S A. 2013;110(23):9469-74.

39. Yamazaki M, Fukushima H, Shin M, Katagiri T, Doi T, Takahashi T, et al. Tumor necrosis factor alpha represses bone morphogenetic protein (BMP) signaling by interfering with the DNA binding of Smads through the activation of NF-kappaB. J Biol Chem. 2009;284(51):35987-95.

40. Hofmann MA, Drury S, Fu C, Qu W, Taguchi A, Lu Y, et al. RAGE mediates a novel proinflammatory axis: a central cell surface receptor for S100/calgranulin polypeptides. Cell. 1999;97(7):889-901.

41. Ogawa N, Yamaguchi T, Yano S, Yamauchi M, Yamamoto M, Sugimoto T. The combination of high glucose and advanced glycation end-products (AGEs) inhibits the mineralization of osteoblastic MC3T3-E1 cells through glucose-induced increase in the receptor for AGEs. Horm Metab Res. 2007;39(12):871-5.

42. Zhou Z, Immel D, Xi CX, Bierhaus A, Feng X, Mei L, et al. Regulation of osteoclast function and bone mass by RAGE. J Exp Med. 2006;203(4):1067-80.

43. Lee Y, Hyung SW, Jung HJ, Kim HJ, Staerk J, Constantinescu SN, et al. The ubiquitin-mediated degradation of Jak1 modulates osteoclastogenesis by limiting interferon-beta-induced inhibitory signaling. Blood. 2008;111(2):885-93.

44. Ryu J, Kim HJ, Chang EJ, Huang H, Banno Y, Kim HH. Sphingosine 1-phosphate as a regulator of osteoclast differentiation and osteoclast-osteoblast coupling. EMBO J. 2006;25(24):5840-51.

45. Oh JE, Kim HJ, Kim WS, Lee ZH, Ryoo HM, Hwang SJ, et al. PlexinA2 mediates osteoblast differentiation via regulation of Runx2. J Bone Miner Res. 2012;27(3):552-62.

46. Edgar R, Domrachev M, Lash AE. Gene Expression Omnibus: NCBI gene expression and hybridization array data repository. Nucleic Acids Res. 2002;30(1):207-10.

47. Barrett T, Wilhite SE, Ledoux P, Evangelista C, Kim IF, Tomashevsky M, et al. NCBI GEO: archive for functional genomics data sets--update. Nucleic Acids Res. 2013;41(Database issue):D991-5.

48. Kim JY, Lee EY, Lee EB, Lee YJ, Yoo HJ, Choi J, et al. Atorvastatin inhibits osteoclastogenesis by decreasing the expression of RANKL in the synoviocytes of rheumatoid arthritis. Arthritis Res Ther. 2012;14(4):R187.

49. Franzoso G, Carlson L, Xing L, Poljak L, Shores EW, Brown KD, et al. Requirement for NF-kappaB in osteoclast and B-cell development. Genes Dev. 1997;11(24):3482-96.

50. Gibbs FE, Barraclough R, Platt-Higgins A, Rudland PS, Wilkinson MC, Parry EW. Immunocytochemical distribution of the calcium-binding protein p9Ka in normal rat tissues: variation in the cellular location in different tissues. J Histochem Cytochem. 1995;43(2):169-80.

51. Senolt L, Grigorian M, Lukanidin E, Michel BA, Gay RE, Gay S, et al. S100A4 (Mts1): is there any relation to the pathogenesis of rheumatoid arthritis? Autoimmun Rev. 2006;5(2):129-31.

52. Wang L, Wang X, Liang Y, Diao X, Chen Q. S100A4 promotes invasion and angiogenesis in breast cancer MDA-MB-231 cells by upregulating matrix metalloproteinase-13. Acta biochim Pol. 2012;59(4):593-8.

53. Wu Y, Liu J, Feng X, Yang P, Xu X, Hsu HC, et al. Synovial fibroblasts promote osteoclast formation by RANKL in a novel model of spontaneous erosive arthritis. Arthritis Rheum. 2005;52(10):3257-68.

54. Nakano K, Okada Y, Saito K, Tanaka Y. Induction of RANKL expression and osteoclast maturation by the binding of fibroblast growth factor 2 to heparan sulfate proteoglycan on rheumatoid synovial fibroblasts. Arthritis Rheum. 2004;50(8):2450-8.

55. Lee HY, Jeon HS, Song EK, Han MK, Park SI, Lee SI, et al. CD40 ligation of rheumatoid synovial fibroblasts regulates RANKL-mediated osteoclastogenesis: evidence of NF-kappaB-dependent, CD40-mediated bone destruction in rheumatoid arthritis. Arthritis Rheum. 2006;54(6):1747-58.

56. Gilbert L, He X, Farmer P, Boden S, Kozlowski M, Rubin J, et al. Inhibition of osteoblast differentiation by tumor necrosis factor-alpha. Endocrinology. 2000;141(11):3956-64.

57. Gilbert L, He X, Farmer P, Rubin J, Drissi H, van Wijnen AJ, et al. Expression of the osteoblast differentiation factor RUNX2 (Cbfa1/AML3/Pebp2alpha A) is inhibited by tumor necrosis factor-alpha. J Biol Chem. 2002;277(4):2695-701.

58. Kaneki H, Guo R, Chen D, Yao Z, Schwarz EM, Zhang YE, et al. Tumor necrosis factor promotes Runx2 degradation through up-regulation of Smurf1 and Smurf2 in osteoblasts. J Biol Chem. 2006;281(7):4326-33.

59. Jang WG, Jeong BC, Kim EJ, Choi H, Oh SH, Kim DK, et al. Cyclic AMP Response Element-binding Protein H (CREBH) Mediates the Inhibitory Actions of Tumor Necrosis Factor alpha in Osteoblast Differentiation by Stimulating Smad1 Degradation. J Biol Chem. 2015;290(21):13556-66.

60. Mah SJ, Lee J, Kim H, Kang YG, Baek SH, Kim HH, et al. Induction of S100A4 in periodontal ligament cells enhances osteoclast formation. Arch Oral Biol. 2015;60(9):1215-21.

61. Cerezo LA, Remakova M, Tomcik M, Gay S, Neidhart M, Lukanidin E, et al. The metastasis-associated protein S100A4 promotes the inflammatory response of mononuclear cells via the TLR4 signalling pathway in rheumatoid arthritis. Rheumatology (Oxford, England). 2014;53(8):1520-6.

62. Herwig N, Belter B, Wolf S, Haase-Kohn C, Pietzsch J. Interaction of extracellular S100A4 with RAGE prompts prometastatic activation of A375 melanoma cells. J Cell Mol Med. 2016;20(5):825-35.

63. Medapati MR, Dahlmann M, Ghavami S, Pathak KA, Lucman L, Klonisch T, et al. RAGE Mediates the Pro-Migratory Response of Extracellular S100A4 in Human Thyroid Cancer Cells. Thyroid. 2015;25(5):514-27.

64. Siddique HR, Adhami VM, Parray A, Johnson JJ, Siddiqui IA, Shekhani MT, et al. The S100A4 Oncoprotein Promotes Prostate Tumorigenesis in a Transgenic Mouse Model: Regulating NFkappaB through the RAGE Receptor. Genes Cancer. 2013;4(5-6):224-34.

65. Saleem M, Kweon MH, Johnson JJ, Adhami VM, Elcheva I, Khan N, et al. S100A4 accelerates tumorigenesis and invasion of human prostate cancer through the transcriptional regulation of matrix metalloproteinase 9. Proc Natl Acad Sci U S A. 2006;103(40):14825-30.

66. Lacey DL, Boyle WJ, Simonet WS, Kostenuik PJ, Dougall WC, Sullivan JK, et al. Bench to bedside: elucidation of the OPG-RANK-RANKL pathway and the development of denosumab. Nat Rev Drug Discov. 2012;11(5):401-19.

67. Drissi H, Sanjay A. The Multifaceted Osteoclast; Far and Beyond Bone Resorption. J Cell Biochem. 2016;117(8):1753-6.

68. Guise TA. Parathyroid hormone-related protein and bone metastases. Cancer. 1997;80(8 Suppl):1572-80.

69. Yang J, Weinberg RA. Epithelial-mesenchymal transition: at the crossroads of development and tumor metastasis. Dev Cell. 2008;14(6):818-29.

70. Thiery JP, Sleeman JP. Complex networks orchestrate epithelial-mesenchymal transitions. Nat Rev Mol Cell Biol. 2006;7(2):131-42.

71. Jin R, Sterling JA, Edwards JR, DeGraff DJ, Lee C, Park SI, et al. Activation of NF-kappa B signaling promotes growth of prostate cancer cells in bone. PLoS One. 2013;8(4):e60983.

72. Odero-Marah VA, Wang R, Chu G, Zayzafoon M, Xu J, Shi C, et al. Receptor activator of NF-kappaB Ligand (RANKL) expression is associated with epithelial to mesenchymal transition in human prostate cancer cells. Cell Res. 2008;18(8):858-70.

73. Grigorian M, Andresen S, Tulchinsky E, Kriajevska M, Carlberg C, Kruse C, et al. Tumor suppressor p53 protein is a new target for the metastasis-associated Mts1/S100A4 protein: functional consequences of their interaction. J Biol Chem. 2001;276(25):22699-708.

74. Li ZH, Bresnick AR. The S100A4 metastasis factor regulates cellular motility via a direct interaction with myosin-IIA. Cancer Res. 2006;66(10):5173-80.

국문초록

류마티스성 관절염과 골 전이암 발병에서의 S100A4의 역할

서울대학교 대학원 세포및발생생물학 전공

(지도교수: 김홍희)

김해민

S100A4 라는 단백질은 S100 칼슘 결합 족 중 하나로써 관절염 및 암에서 그 역할이 점차 밝혀지고 있다. 더하여 관절염과 골전이 암은 골의 파괴를 수반 한다. 최근 연구들에 따르면 S100A4 는 암전이와 류마티스성 관절염에서의 주요 인자로써 주목 받고 있다. 하지만 아직까지 S100A4 와 골 항상성에 대해 학계에 보고된 바가 없기에 본 연구를 진행 하였다. 본 연구에서는 ELISA 를 통해 류마티스성 관절염

환자의 관절액에서 높은 양의 S100A4 가 발현 된다는 것을 확인 하였다. GEO 검색을 통해 류마티스성 관절염 환자들이 TNF-alpha inhibitor 치료를 받더라도 높은 양의 S100A4 를 발현 한다는 것을 확인 하였다. 더하여 또 다른 GEO 검색을 통해 유방암 골 전이 환자들이 높은 양의 S100A4 를 발현 한다는 것을 확인하고 면역결핍 쥐를 이용한 유방암 및 전립선암 골 전이 모델에서도 암세포가 골로 전이되면 높은양의 S100A4 를 발현 한다는 것을 확인 하였다.

본 연구에서는 세포 밖의 S100A4 즉 세포로부터 흘러나온 S100A4가 생체 내 혹은 실험관 내에서 골 부피를 줄일 수 있다는 것을 확인 하였다. 이러한 원인은 분화 및 기능이 증가된 파골 세포와 기능이 감소된 조골 세포에 의한 것임을 확인 하였다. 본 연구에서는 파골세포의 RAGE라는 수용체가 S100A4를 받아들여 파골세포 내의 NF-kB 신호체계가 활성화 됨을 확인 하였다. 더하여 조골세포 내의 NF-kB 신호체계 역시 S100A4에 의해 활성화 되며 이는 미네랄화를 저해 시킴을 확인

하였다. 추가적으로 류마티스성 관절염 환자의 활막섬유모세포가 S100A4에 의해 RANKL이라는 강력한 파골세포 활성 인자를 발현 할 수 있음을 확인 하였다. 종합적으로 세포 밖 S100A4라는 단백질은 류마티스성 관절염 및 골 전이 암 환경에서 골 항상성을 무너뜨리며 해당 질병의 훌륭한 치료 타겟으로 사료 된다.

주요어: S100A4, 파골세포, 조골세포, 골 전이, 류마티스성 관절염

학번: 2015-30621